RESEARCH IN SEISMOLOGY

William Stauder

Saint Louis University

Prepared for:

Advanced Research Projects Agency
Air Force Office of Scientific Research

1974

Semi-Annual Technical Report
May 1 - October 31, 1974

ARPA Order No.: 1827-5
Program Code: 3F10
Contractor: Saint Louis University
Effective Date of Contract: 1 March 1973
Contract Expiration Date: April 30, 1975
Amount of Contract: $103,340
Contract Number: F44620-73-C-0042
Principal Investigator: William Stauder
Phone: 314-535-3300-Ext. 540
Program Manager: Same
Short Title: Research in Seismology

Sponsored by

Advanced Research Projects Agency

ARPA Order No. 1827-5

REPORT DOCUMENTATION PAGE

READ INSTRUCTIONS BEFORE COMPLETING FORM

1. REPORT NUMBER: AFOSR - TR 75 - 0265	2. GOVT ACCESSION NO.
3. RECIPIENT'S CATALOG NUMBER: AD/A-005665	
4. TITLE (and Subtitle): RESEARCH IN SEISMOLOGY	5. TYPE OF REPORT & PERIOD COVERED: Semi-Annual Technical, 1 May - 31 Oct 74
	6. PERFORMING ORG. REPORT NUMBER
7. AUTHOR(s): William Stauder	8. CONTRACT OR GRANT NUMBER(s): F44620-73-C-0042
9. PERFORMING ORGANIZATION NAME AND ADDRESS: St Louis University, Department of Earth and Atmospheric Sciences, St Louis, MO 63156	10. PROGRAM ELEMENT, PROJECT, TASK AREA & WORK UNIT NUMBERS: 62701E, AO 1827-5
11. CONTROLLING OFFICE NAME AND ADDRESS: Advanced Research Projects Agency, NMR, 1400 Wilson Boulevard, Arlington, VA 22209	12. REPORT DATE: 1974
	13. NUMBER OF PAGES: 68
14. MONITORING AGENCY NAME & ADDRESS (if different from Controlling Office): Air Force Office of Scientific Research/NP, 1400 Wilson Boulevard, Arlington, VA 22209	15. SECURITY CLASS. (of this report): Unclassified
	15a. DECLASSIFICATION/DOWNGRADING SCHEDULE

16. DISTRIBUTION STATEMENT (of this Report)

Approved for distribution: distribution unlimited.

17. DISTRIBUTION STATEMENT (of the abstract entered in Block 20, if different from Report)

18. SUPPLEMENTARY NOTES

19. KEY WORDS (Continue on reverse side if necessary and identify by block number)

Lg phase
Intra-plate earthquakes
Corner period

20. ABSTRACT (Continue on reverse side if necessary and identify by block number)

The investigations under study in this project pertain to the properties of sources within continental interior regions and of shallower focus thrust faults near the borders of plates as these affect the radiation pattern of seismic waves, and the attenuation structure of continental shields, plateaus, and younger tectonic provinces along typical paths from such sources. Both areas of study are related to the amplitude of seismic waves and magnitude determination.

Research in Seismology

Semi-Annual Technical Report

Contract F44620-73-C-0042

Table of Contents

Technical Report Summary

An examination of the spectral characteristics of the Lg phase for intra-plate earthquakes in North America shows a uniform relationship between the corner period and the seismic moment. This implies a uniformity of earthquake processes in the central United States over a wide range of event sizes. Using reduced spectra a method has been outlined for relating magnitude observations at periods other than 1 second to m_b.

Multi-mode theory is applied to computing ground motion time histories. Agreement between predicted and observed ground motion shows the method to be excellent over a distance range of 100 to 2000 kilometers. A comparison of predicted ground motions computed for a stable continental interior model and for an active model shows that effects of the difference in the attenuation models are seen at distances greater than 100 kilometers for periods greater than 1.5 seconds.

Values of the attenuation coefficient for Rayleigh waves of period 5 to 40 seconds have been determined for various paths across North America from the nuclear events Rulison and Rio Blanco. Application of a Backus-Gilbert inversion method showed the quality factor values in the upper crust of the western Cordillera are about half those of the upper crust in eastern North America. Low velocity surface sediments strongly affect the attenuation at periods less than 5 seconds. Similar studies applied to surface wave traversing Eurasian paths are being used as a tool to determine attenuation differences by tectonic provinces in this region.

Semi-Annual Technical Report

Introduction

The investigations under study in this project pertain to the properties of sources within continental interior regions and of shallower focus thrust faults near the borders of plates as these affect the radiation pattern of seismic waves, and the attenuation structure of continental shields, plateaus, and younger tectonic provinces along typical paths from such sources. Both areas of study are related to the amplitude of seismic waves and magnitude determination.

Previous Technical Reports have presented a study of the M_S vs m_b relation for central U. S. earthquakes, a technique for determining earthquake source parameters by using surface wave amplitude spectra, the seismic scaling law and source mechanism characteristics for small magnitude events in the central U.S. and the Q structure above the subduction zone in South America.

The Report for the present period will concern spectral characteristics of short period surface waves in continental interiors, the Q structure of the North American and Eurasian continents, and the radiation from shallow thrust faults in eastern Siberia-Kurile Islands. The Report will include both work that has been completed and that in progress.

A. Work Completed During the Report Period.

Work completed during this six month report period has been presented in four papers which have been submitted for publication.

R. L. Street, R. B. Herrmann, and O. W. Nuttli, Spectral Characteristics of the Lg Wave Generated by Central United States Earthquakes, accepted for publication in the Geophysical Journal.

R. B. Herrmann and O. W. Nuttli, Ground Motion Modelling at Regional Distances for Earthquakes in a Continental Interior, I. Theory and Observations, accepted for publication in Earth Engineering and Structural Dynamics.

R. B. Herrmann and O. W. Nuttli, Ground Motion Modelling at Regional Distances for Earthquakes in a Continental Interior, II. Effect of Focal Depth, Azimuth and Attenuation, accepted for publication in Earth Engineering and Structural Dynamics.

B. J. Mitchell, Regional Rayleigh Wave Attenuation in North America, submitted to J. Geophys. Res.

A digest, or presentation of aspects of these papers most immediately of interest to project goals follows.

A.1. Spectral Characteristics of the Lg Wave Generated by Central U. S. Earthquakes.

by R. L. Street, R. B. Herrmann, and O. W. Nuttli

For many earthquakes the S phase is not a distinct arrival, but is associated with other arrivals of body and surface waves. The theory of Brune (1970, 1971) and of Savage (1972) have not

approached the problem of estimating source parameters from such a complicated set of arrivals. The objective of this study is to accomplish this task.

The events studied occurred in the central U. S. between 1961 and mid 1974 and fall in the magnitude range $0.5 \leq m_b \leq 5.3$. Sixty three seismograph stations, all part of the WWSSN, LRSM, Saint Louis University, or independent networks, provided Lg observations for one or more of the events studied. In each case the instrument-corrected spectra of the ground motion were used for analysis only in the pass band for which the instrument response was greater than one-tenth the maximum response. In the digitizing of the seismograms the resolution attainable depended on the time rate of the record. LRSM short period seismograms, when viewed through a 10X viewer, were found to give good spectral results at periods as short as 0.1 seconds. WWSSN type data were useful down to periods of 0.3 seconds. Records were generally digitized from the time of the maximum trace offset associated with the Sg or Lg arrival until the signal reached the background noise level.

Sample displacement spectral densities are shown in Figures 1 and 2. For both events the spectrum is flat at the long period end and falls off at very short periods as T^2 (or ω^{-2}). For some events, such as that of July 23, 1962 (Figure 2), an intermediate ω^{-1} trend was observed.

The shape of the Lg spectrum in Figures 1 and 2 is similar to that predicted by Brune (1970). However, some different interpretations of the spectra are required since body wave theory no longer is applicable over the propagation paths in question

and since the Lg phase is not a clear S wave but most likely a superposition of higher mode surface waves.

A model was selected which properly corrects the Lg spectrum for geometrical spreading and at the same time relates the long-period flat portion of the spectrum to the seismic moment M_o. The model chosen relates the Lg spectrum $\Omega(\omega)$ at a distance r from the source to the distance-corrected far-field estimate of the source spectrum $S(\omega)$

$$S(\omega) = \begin{cases} 4\pi\rho\beta^3 r_o \left(\frac{r}{r_o}\right) \Omega(\omega) & , \; r \leq r_o \\ 4\pi\rho\beta^3 r_o \left(\frac{r}{r_o}\right)^{1/2} \Omega(\omega) & , \; r \geq r_o \end{cases} \qquad (1)$$

Here r_o serves two functions. First, r_o adjusts the scaling so that $S(\omega = o) = M_o$. Secondly, r_o establishes a distance which marks the change in the character of the geometrical spreading of the Lg wave train from that of typically body-wave at near distances to typically surface-wave at large distances.

The values adopted for the parameters in equation (1) are ρ = 2.5 gm/cm^3, β = 3.5 km/sec, and r_o = 100 km. The value chosen for r_o is that which was found, empirically, to give stable values of M_o as equation (1) is evaluated at various distances r.

Equation (1) was applied to the spectra obtained from seventy-eight earthquakes in the central U.S. For each event average values of the seismic moment and corner periods were determined from the distance-corrected spectra. Figure 3 presents the general features of the Lg source spectra estimates for representative of these events. It is noted that for events with seismic moments less than 10^{20} dyne^{-cm}, no ω^{-1} trend is observed. For events with greater seismic moments, ω^{-1} trends are noted in

some instances.

Figure 4 is a plot of the T_{o2} corner period versus seismic moment, where T_{o2} is the corner period between the ω^o and ω^{-2} spectral trends (for spectra containing both a T_{o1} and a T_{12} corner, the mean of these two is taken as T_{o2}). The average trend of the corner period is indicated by the straight line segments. Special features of this plot include a) the consistent relationship between the corner period and the seismic moment, M_o, and b) the kink in the corner period vs M_o curve for seismic moments between 10×10^{21} and 5×10^{21} dyne-cm.

Several conclusions follow from the features that are noted in the plots of Figures 3 and 4.

1. The consistent relationship between T_{o2} and M_o mark a characteristic of earthquakes of the central U.S. No such relation is found in southern California where wide ranges in stress drop introduce a wide variation in corner period for a given value of seismic moment (Thatcher and Hanks, 1973).
2. The kink in the corner period is a characteristic of Aki's (1972) revised model A. On the other hand, the relation of M_o to the cube of the corner period, in regions excluding the kink, is a characteristic of Aki's models A and B, but not his revised model A.
3. Brune (1970, 1971) has derived a relation between the corner period T_{o2} of SH waves and the source dimension whereby under conditions of constant stress drop the seismic moment varies as the cube of the corner period.

The same relation applied to the Lg spectra of Figure 3 imply that in the central U.S. earthquakes with M_o less than 10^{21} dyne-cm are characterized by a stress drop of about 1 bar, those with M_o between 5×10^{21} and 10^{23} dyne-cm by a stress drop of about 6 bars. The kink in Figure 4 marks a transition between the two.

4. In Figure 3, in terms of Brune's (1970) distinction between complete and partial stress drop, in the central U.S. events with seismic moment less than 3×10^{20} dyne-cm exhibit only an ω^{-2}, or complete stress drop, whereas some of the large events exhibit also an ω^{-1} or partial stress drop.

Finally, from the reduced spectra of Figure 3 we can relate m_b (1 second) to magnitude observations at periods other than 1 second. In general, the equation for magnitude for a particular range of applicability is of the form (Nuttli, 1972)

$$m_T = B(T) + C(T,D) \log_{10}(D) + \log_{10}(A/T) \qquad (2)$$

where D is epicentral distance and A is the maximum sustained ground displacement at period T of a given wave type. The coefficient C corrects for geometric spreading and attenuation, the factor B scales the formula to source reference level. Assuming that the magnitude defined for a given period T is directly related to $\log_{10} S(\omega)$, a relationship between a magnitude scale at period T and some other period T' can be established by comparing the relative levels of $S(\omega)$ at the two periods.

For example, from Figure 3, in comparing spectra with $M_o = 10^{20}$ dyne-cm to $M_o = 10^{21}$ dyne-cm, we would expect a 1.0 unit change in M_s (20 second period) or in m_b (1 second) but a 0.7 unit change in magnitude $m_{0.3}$ based on a 0.3 second LG component. Similarly there will be a 0.7 unit change in $m_{0.1}$ based on a 0.1 second component. A scaling law can thus be constructed giving the correspondence between M_o, M_S, m_b, $m_{0.3}$ and $m_{0.1}$.

Consequently, in any region such as the central U.S. where source characteristics are found to be highly predictable, a reliable estimate of m_b can be made from signals with periods other than 1 second.

References

Aki, K., 1972. Scaling law of earthquake source time-function, Geophys. J. R. astr. Soc., 31, 3-25.

Brune, J. N., 1970. Tectonic stress and the spectra of seismic shear waves from earthquakes, J. Geophys. Res., 75, 4997-5009.

Brune, J.N., 1971. Correction to 'Tectonic stress and the spectra of seismic shear waves from earthquakes,' J. Geophys. Res., 76, 5002.

Nuttli, O. W., 1972. Magnitude, intensity and ground motion relations for earthquakes in the central United States, Proceedings of the International Conference on Microzonation for Safer Construction Research and Application, Seattle, Oct. 30 - Nov. 3, pp 307-318.

Savage, J. C., 1972. The relation of corner frequency to fault dimensions, J. Geophys. Res., 77, 3788-3795.

Thatcher, W. & Hanks, T. C., 1973. Source parameters of southern California earthquakes, J. Geophys. Res., 78, 8547-8576.

Figure Captions

Figure 1. Spectrum for the earthquake of 02 February 1962, showing the T_{02} corner between the ω^0 and ω^{-2} asymptotic trends of the spectrum.

Figure 2. Spectrum for the earthquake of 23 July 1962, showing the T_{01} corner between the ω^0 and ω^{-1} trends and the T_{12} corner between the ω^{-1} and ω^{-2} trends.

Figure 3. General shape of the Lg estimated source spectra $S(\omega)$.

Figure 4. Plot of the T_{02} corner period as a function of seismic moment.

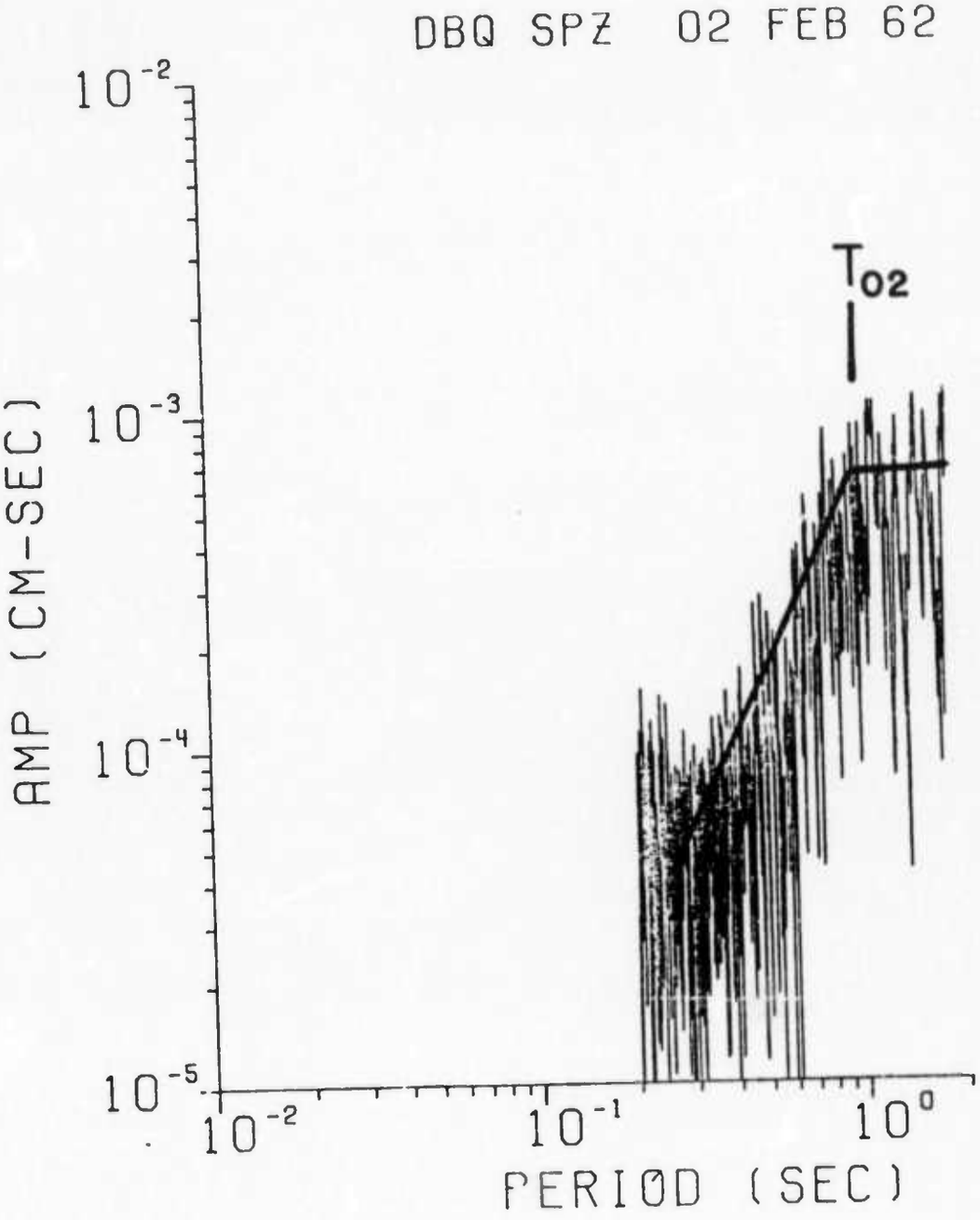
DBQ SPZ 02 FEB 62
10^{-2}
10^{-3}
10^{-4}
10^{-5}
AMP (CM-SEC)
T_{02}
10^{-2}
10^{-1}
10^{0}
PERIOD (SEC)

Figure 1

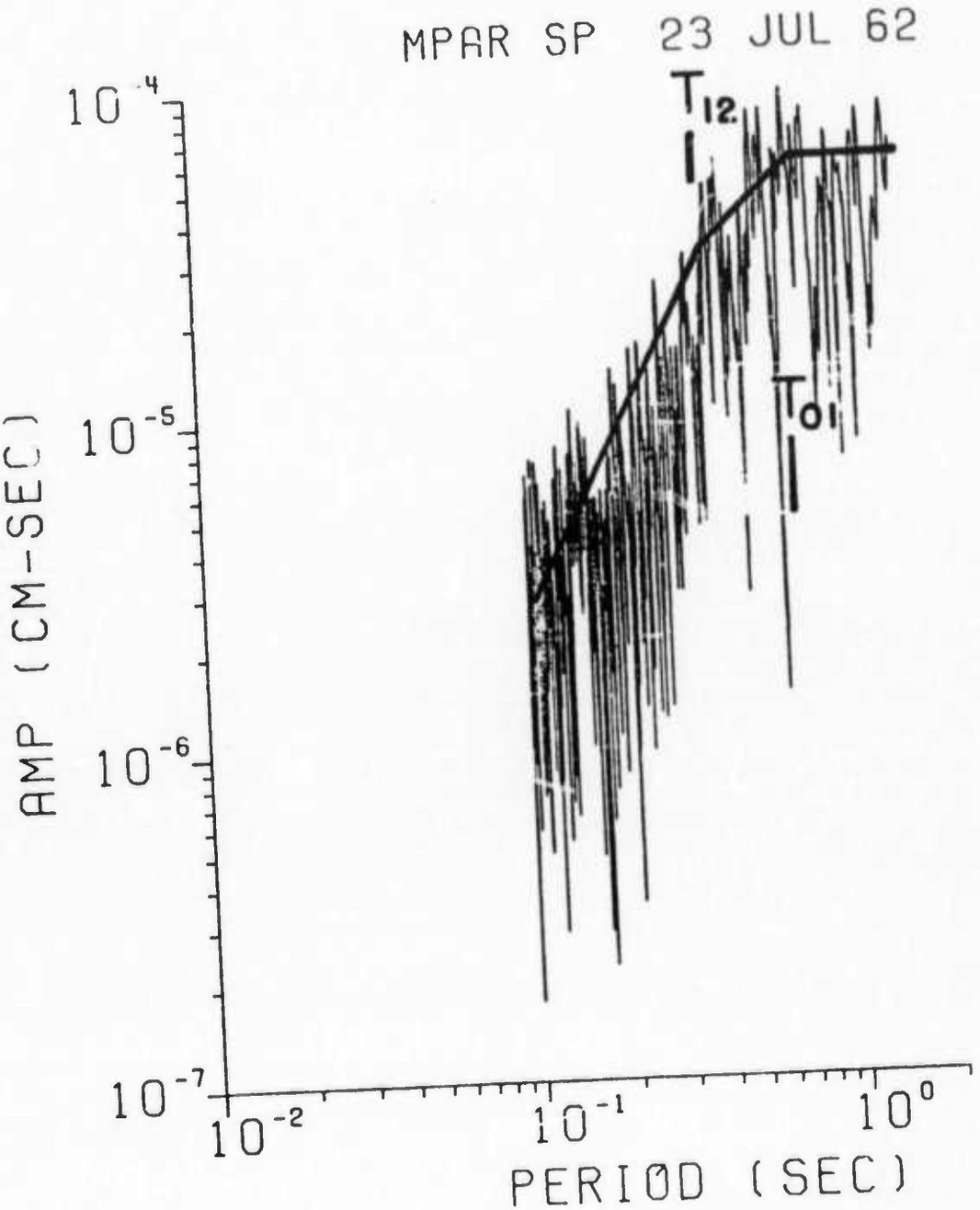
MPAR SP 23 JUL 62
T_{12}
T_{01}
10^{-4}
10^{-5}
10^{-6}
10^{-7}
AMP (CM-SEC)
10^{-2}
10^{-1}
10^{0}
PERIOD (SEC)

Figure 2

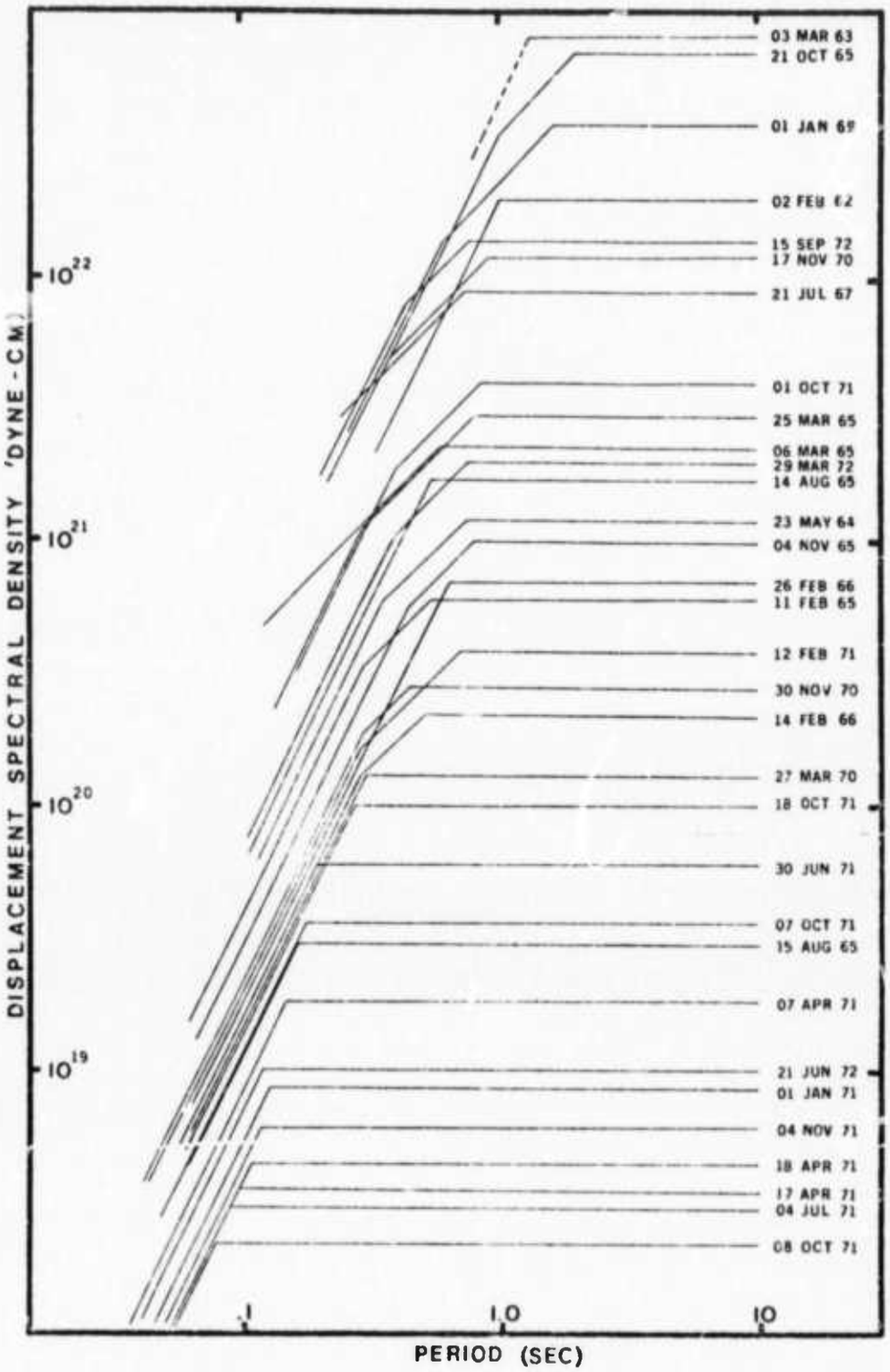
03 MAR 63
21 OCT 65
01 JAN 69
02 FEB 62
15 SEP 72
17 NOV 70
21 JUL 67
01 OCT 71
25 MAR 65
06 MAR 65
29 MAR 72
14 AUG 65
23 MAY 64
04 NOV 65
26 FEB 66
11 FEB 65
12 FEB 71
30 NOV 70
14 FEB 66
27 MAR 70
18 OCT 71
30 JUN 71
07 OCT 71
15 AUG 65
07 APR 71
21 JUN 72
01 JAN 71
04 NOV 71
18 APR 71
17 APR 71
04 JUL 71
08 OCT 71
10^{22}
10^{21}
10^{20}
10^{19}
DISPLACEMENT SPECTRAL DENSITY 'DYNE-CM)
.1
1.0
10
PERIOD (SEC)

Figure 3

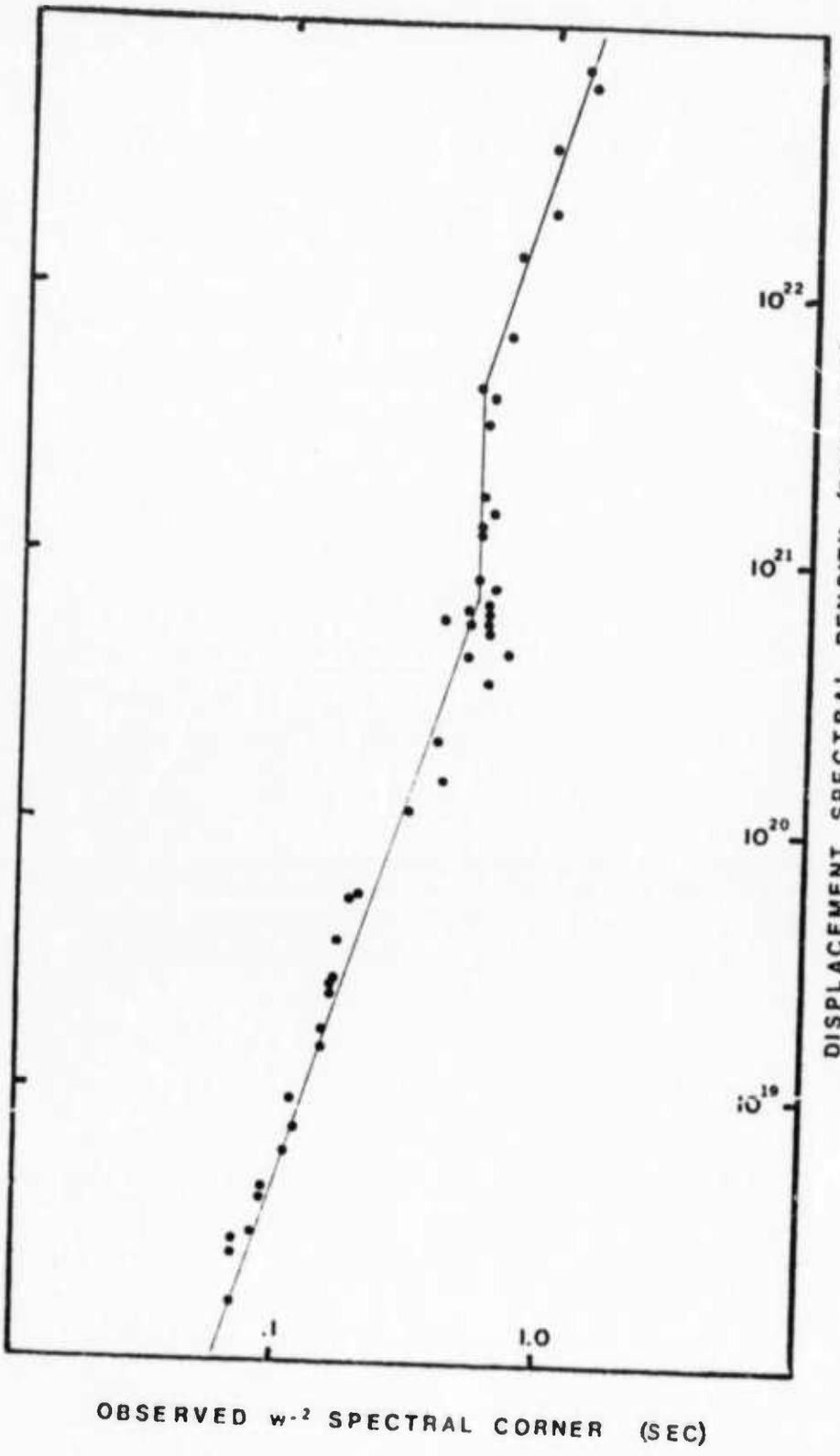
10^{22}
10^{21}
10^{20}
10^{19}
DISPLACEMENT SPECTRAL DENSITY (DYNE-CM)
.1
1.0
OBSERVED w^{-2} SPECTRAL CORNER (SEC)

Figure 4

A. 2. Ground Motion Modelling at Regional Distances for Earthquakes in a Continental Interior

by R. B. Herrmann and O. W. Nuttli

I. Theory and Observations

This study attempts to model the ground motion at regional distances by the superposition of multiple mode surface wave arrivals.

The approach used is based on the equivalence of a dislocation on a fault surface within an elastic isotropic earth model to a double-couple force system acting at the point of application. This equivalency permits one to calculate the theoretical Fourier spectra of the surface-wave displacements, using normal mode surface wave theory, for a dislocation source in a multilayered elastic isotropic medium. The theoretical development and the resulting equations for computing the ground motion are given by Tsai and Aki (1970) and by Levshin and Yanson (1971).

In addition to source parameters, theoretical ground motions depend also on medium effects, such as larger thicknesses, compressional and shear wave velocities, densities, and the frequency-dependent anelastic attenuation coefficients of both fundamental and higher mode surface waves.

Herrmann has shown (1974) that the amplitude spectrum of the surface wave ground displacement of the individual modes is relatively insensitive to perturbations in the velocities or densities of the layered flat-earth model. However, this is not true of the phase spectrum of the ground motion, especially at the higher frequencies. As a consequence it is difficult to

obtain a perfect match between the synthetic seismograms, for which an accurate knowledge of the phase spectrum is required, and the actual seismograms. On the other hand, descriptive properties of the ground motion such as maximum ground velocity and maximum ground acceleration, which depend more on the amplitude spectrum, show excellent agreement between calculated and observed values, as will be demonstrated below.

Following Tsai and Aki (1970), the ground motion displacement of the surface can be represented in the form

$$f(r,t) = \frac{1}{2\pi} S(\omega) \sum_{j=1}^{N(\omega)} A(r,\omega) \exp (i\omega t - ik_j r - \gamma_j r)\, d\omega \quad (1)$$

In this equation, $S(\omega)$ is the Fourier transform of the dislocation time history and $A_j(r,\omega) \exp(- ik_j r)$ is the Fourier transform of the medium impulse response to a point dislocation at the source. $A_j(r,\omega)$ is a function of the faulting geometry source depth, and the elastic properties of the medium. The γ_j coefficient takes into account anelastic transmission properties of the medium. The summation runs over the number of modes present at a given frequency.

The numerical computations involved in determining the $A_j(r,\omega)$ at high frequencies become involved and time consuming due to the lack of numerical accuracy and because the number of modes present at a given frequency is proportional to the frequency. In the earth model considered below we were limited to a period range of 1.5 to 400 seconds for Love waves, which had eight modes present at a period of 1.5 seconds, and to a period range of 2.0 to 400 seconds for Rayleigh waves, which had eight

modes present at a period of 2.0 seconds. To extend the computations into the period range of 0.5 to 1.5 or 2.0 seconds in order to describe the known large surface-wave motions in this period range would have required the use of about thirty surface-wave modes at a period of 0.5 seconds.

Computations

In applying equation (1) a simplified earth model for the central U.S. based on Nuttli et al. (1969), modified to include a low-velocity layer at the surface and a slight low-velocity channel in the crust, was used. The anelastic attenuation model was based on an average of the Rayleigh and Love wave attenuation values determined by Mitchell (1973a,b) and Herrmann (1973,1974), and on the higher-mode short-period Lg values by Nuttli (1973).

Three central U. S. earthquakes, whose source characteristics are given in Table 1, were selected to test the appropriateness of the multiple-mode surface wave theory for modelling ground motions. The parameters given in the table were determined by Herrmann (1974) and by Street and Herrmann (1974).

The source spectrum model is based on the models of Brune (1970) and Aki (1972):

$$S(\omega) = \begin{cases} M_0/(i\omega), & \omega \leq \omega_1 \\ M_0 \omega_1/i\omega^2), & \omega \geq \omega_1 \end{cases} \qquad (2)$$

where ω_1 is the corner frequency. This model adequately describes the Fourier amplitude spectrum of the source time function, but may be in error with respect to the phase information at high frequencies.

Comparison of Predictions and Observations.

In this study we are only modelling surface waves with periods greater than 1.5 seconds. Accordingly, the observational seismograms which we shall present are from the long period instruments of the WWSSN network. These instruments peak at periods of 10 to 30 seconds, and fall off at 6 db per octave at periods less than 10 seconds and 18 db per octave for periods greater than 30 seconds. Therefore the seismogram embraces the ground displacements in the period range of 10 to 30 seconds at the expense of the motion at the shorter and longer periods.

Figure 1 compares the observed and predicted long-period seismograms for the vertical component Rayleigh waves at FLO (Florissant, Missouri) and the Love waves at OXF (Oxford, Mississippi) for an earthquake which occurred near Cairo, Illinois on August 14, 1965. The distances from the epicenter to FLO and OXF are 200 and 300 km, respectively. Note the excellent agreement between the observed and predicted seismograms at OXF with respect to wave form, amplitudes, and signal duration. Likewise the agreement is very good for the Rayleigh wave at FLO. Here the important motion is the pulse-like event near the center of the record. The absence of the shorter-period tail immediately following the large pulse on the predicted seismogram results from too high a value of the anelastic attenuation coefficient for the fundamental mode between 2 and 3 seconds.

Figure 2 compares the observed and predicted Love waves at DUG (Dugway, Utah), at a distance of 2100 km from the southern Illinois earthquake of November 9, 1968. The similarity in the

large amplitude motion is quite good, although the predicted peak amplitudes are only about 80% of the observed. The latter part of the observed seismogram is not accounted for by pure Love waves, and may be due to some Rayleigh-wave interference or multi-path effects.

Another way of comparing the predicted and observed ground motions is to look at simple diagnostic factors, such as maximum ground velocity or acceleration as a function of distance. For this purpose theoretical velocitygrams and accelerograms were generated for various distances and azimuths about the source, using the appropriate source parameters for each event of Table 1. The results are given in the full paper.

In conclusion, multiple-mode surface wave theory has been used effectively to describe ground motion of Love waves at periods greater than 1.5 seconds and of Rayleigh waves at periods greater than 2.0 seconds. We feel confident of being able to predict ground motions at distances greater than 100 km from the sources on the basis of this theory, given a suitable model of the earthquake.

II. Effect of Focal Depth, Azimuth and Attenuation.

In further development of the ground motion studies an investigation has been made of the effects of focal depth, azimuth from the source, and of attenuation on the calculation of theoretical ground motion.

Using the same crustal model and source time function as in Part I, two anelastic attenuation models were constructed: a <u>stable</u> model appropriate to a geologically stable region such as

the central or eastern U.S., and an active model constructed so as to be characteristic of an active region such as southern California. At shorter periods these models use the anelastic attenuation coefficients of the 1-second Lg wave estimated by Nuttli (1973) for the central U.S. and for southern California. For periods greater than 10 seconds both models are assumed equal and are based on Mitchell (1973a,b) and Herrmann (1973,1974), as in Part I.

For the source model, only one particular fault type is considered, a pure thrust type motion on a fault striking north-south and dipping 45° to the east or west. From Tsai and Aki (1970), for this source configuration the Rayleigh spectral amplitude will vary with azimuth φ as

$$A + B \cos 2\varphi \qquad (1)$$

where A and B are functions dependent on focal depth, mode, and frequency. The radiation pattern at a given period and mode may be circular, elliptical, or a two or four-leaved rose, or combination of these. The azimuthal dependence of the Love wave is

$$C \sin 2\varphi \qquad (2)$$

where C is a similar function dependent on depth mode or frequency. Here the radiation pattern is always a four-leaved rose.

The effect of focal depth on the amplitude spectrum of Love waves at a distance of 1000 km along an azimuth of 45° is shown in Figure 3. The solid curve is the amplitude spectrum for a source depth of 2.5 km, the dashed curve for 19.5 km. But the difference in focal depth causes a profound change in the Love

wave excitation at short periods. The shallower event will excite the shorter periods about five times more than the deeper event.

Figure 4 shows the effect of focal depth for Rayleigh waves. The spectral hole at 6 second period for h = 2.5 km, and at 40 seconds for h = 19.5 are characteristic of the choice of fault type modeled (Tsai and Aki, 1970). Similarly as for Love waves, the short period excitation is about five times greater for the shallow event than for the deeper.

The effect of the stable and active attenuation models on the ground displacements of the Love wave at distances of 50 to 500 km along an azimuth of 45° for a source at depth 9.5 km is shown in Figure 5. Differences arising from the attenuation model are not measurable at distances less than 100 km. This is for the periods 2 seconds and greater of our caluclations. At large distances the shorter periods are attenuated notably more by the active model than by the stable.

Figure 6 compares the effects of the two attenuation models on the vertical component Rayleigh wave ground displacements. The Rayleigh displacements are not as impulsive as the Love wave values. But the effects of the different attenuation models are similar in the sense that the active model filters out short period components at distances greater than 100 km.

Ground velocities and accelerations for both Love and Rayleigh wave motion have also been computed and compared for the two attenuation models.

The effect focal depth is further examined for Love and Rayleigh wave displacements and velocities in Figures 7 and 8,

respectively. The motions shown were generated at a distance of 250 km from the source along an azimuth of 45°, and for focal depths of 2.5, 9.5, and 19.5 km. As might be expected from the spectra of Figures 3 and 4, the short period excitation is strongly dependent on focal depth. Note also that a shallow event has a longer signal duration than a deeper event, due primarily to a greater excitation of the fundamental mode waves at short periods which in turn have lower group velocities than the higher mode waves at the same period (Panza et al., 1973).

For the particular source geometry in question, no notable effect of azimuth, other than variation in relative amplitude, is found.

References

Aki, K., Scaling law of earthquake time function, Geophys. J. 31, 3-26 (1972).

Brune, J. N., Tectonic stress and the spectra of seismic shear waves from earthquakes, J. Geophys. Res. 75, 4997-5009 (1970).

Herrmann, R. B., Surface-wave generation by the south central Illinois earthquake of November 9, 1968, Bull. Seism. Soc. Am. 63, 2121-2134 (1973).

Herrmann, R. B., Surface wave generation by central United States earthquakes, Ph.D. Dissertation, Saint Louis University (1974).

Levshin, A.L. and Z. A. Yanson, Surface waves in vertically and radially inhomogeneous media, Algorithms for the Interpretation of Seismic Data (vol. 5 of the series Computational

Seismology, V. I. Keilis-Borok, Editor) Nauka Press, Moscow, 147-177 (in Russian) (1971).

Mitchell, B. J., Radiation and attenuation of Rayleigh waves from the southeastern Missouri earthquake of October 21, 1965, J. Geophys. Res. 78, 886-899 (1973).

Mitchell, B. J., Surface-wave attenuation in central North America, Bull. Seism. Soc. Am. 63, 1057-1071 (1973).

Nuttli, O. W., W. Stauder, and C. Kisslinger, Travel time tables for earthquakes in the central United States, Earthquake Notes 40, 19-28 (1969).

Panza, G. F., F. A. Schwab and L. Knopoff, Multimode surface waves for selected focal mechanisms-- I. Dip-slip sources on a vertical fault plane, Geophys. J. 34, 265-278 (1973).

Street, R. L., and R. B. Herrmann, Earthquake mechanics in southeast Missouri and adjacent areas, (abstract) meeting of Seismological Society of America at Las Vegas, Nevada (1974).

Tsai, Y. B. and K. Aki, Precise focal depth determination from amplitude spectra of surface waves, J. Geophys. Res. 75, 5729-5743 (1970).

Table 1. Source Characteristics

Date	Origin Time (UT)	Lat. (°)	Long. (°)	Strike (°)	Dip (°)	Slip (°)	m_b	M_o dyne-cm	l sec^{-1}	H (km)
14 Aug 65	13 13 56.6	37.2	89.3	20	70E	200	3.8	1.4E21	12.5	1
21 Oct 65	02 04 38.3	37.5	91.0	54	53S	254	4.9	6.9E22	3.1	5
09 Nov 68	17 01 42.0	38.0	88.5	359	47E	78	5.5	9.0E23	1.5	20

Figure Captions

Figure 1. Comparison of observed and predicted waveforms recorded on the OXF and FLO long-period instruments for the earthquakes of 14 August 1965.

Figure 2. Comparison of the observed and predicted Love waves on the DUG long-period seismograph for the earthquake of 9 November 1968.

Figure 3. Love wave amplitude spectra for focal depths of 2.5 km (solid curve) and 19.5 km (dashed curve).

Figure 4. Rayleigh wave amplitude spectra for focal depths of 2.5 km (solid curve) and 19.5 km (dashed curve).

Figure 5. Love wave displacement time histories as a function of distance and attenuation model for a focal depth of 9.5 km and receiver azimuth of 45°. Displacements are in cm.

Figure 6. Rayleigh wave displacement time histories as a function of distance and attenuation model for a focal depth of 9.5 km and a receiver azimuth of 45°.

Figure 7. Effect of focal depth variation on Love wave displacements and velocities for the stable attenuation model at a distance of 250 km and an azimuth of 45° from the source.

Figure 8. Effect of focal depth variation on Rayleigh wave displacements and velocities for the stable attenuation model at a distance of 250 km and at an azimuth of 45° from the source.

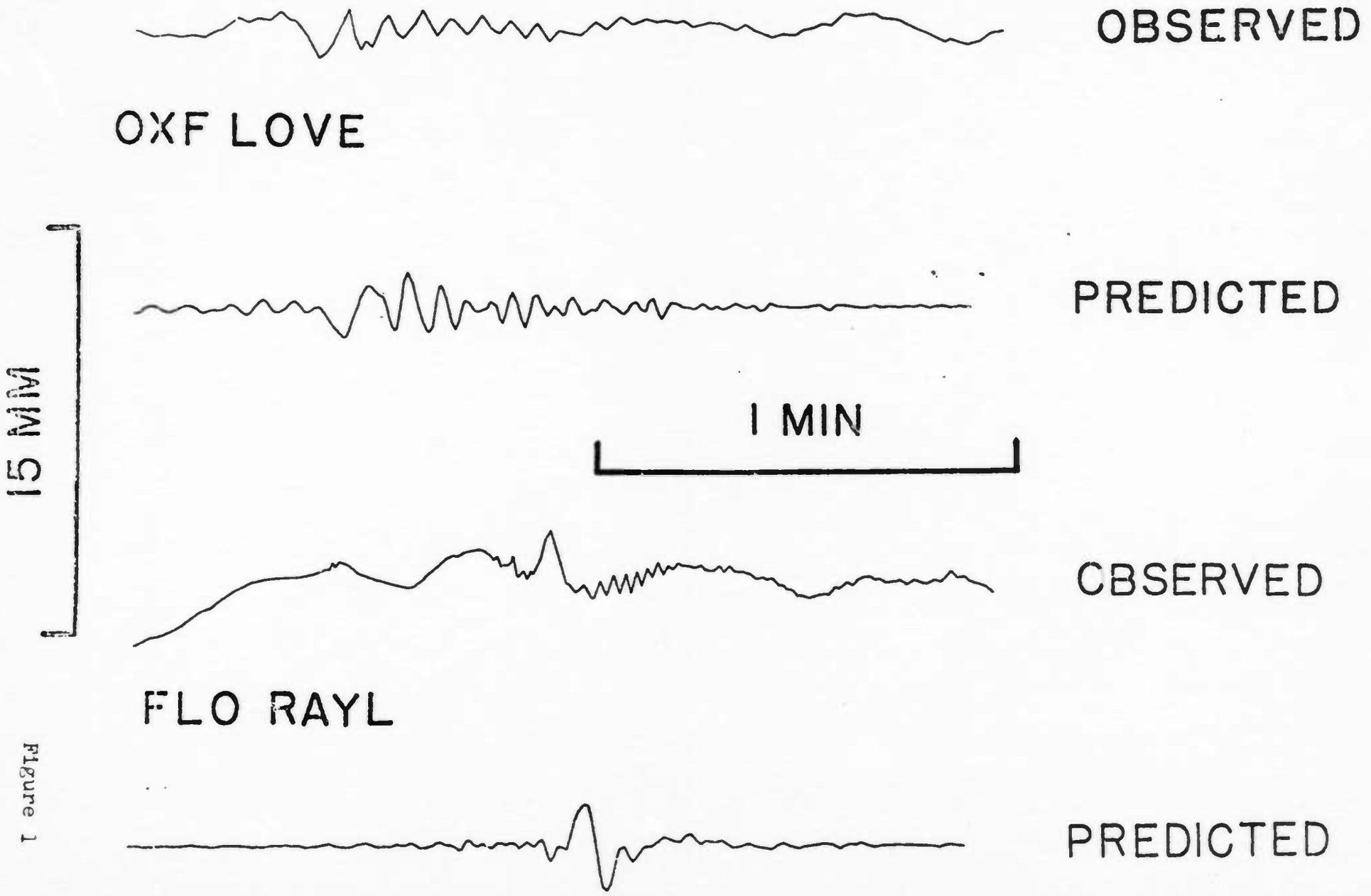
OBSERVED
OXF LOVE
PREDICTED
15 MM
1 MIN
OBSERVED
FLO RAYL
PREDICTED

Figure 1

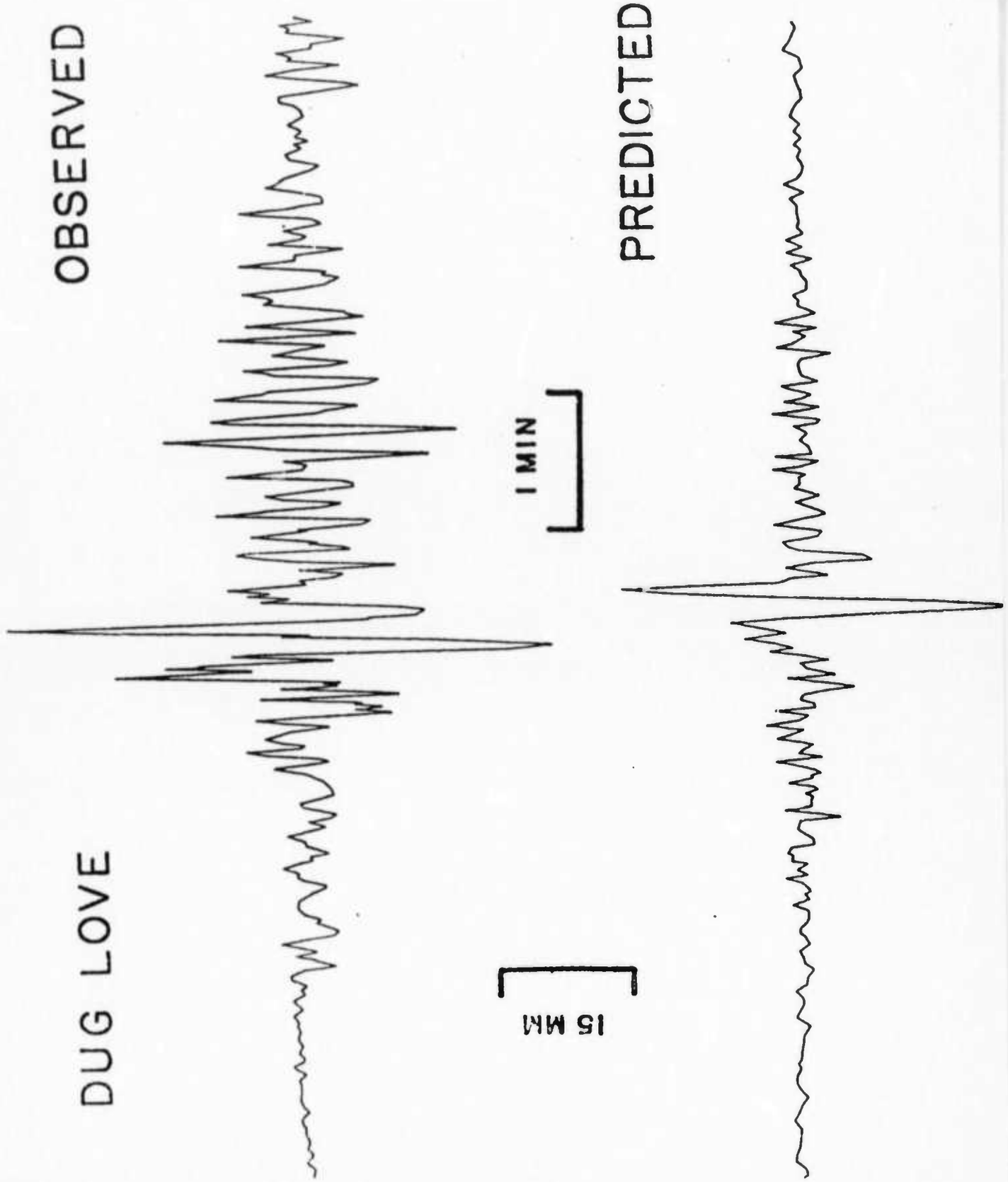

Figure 2

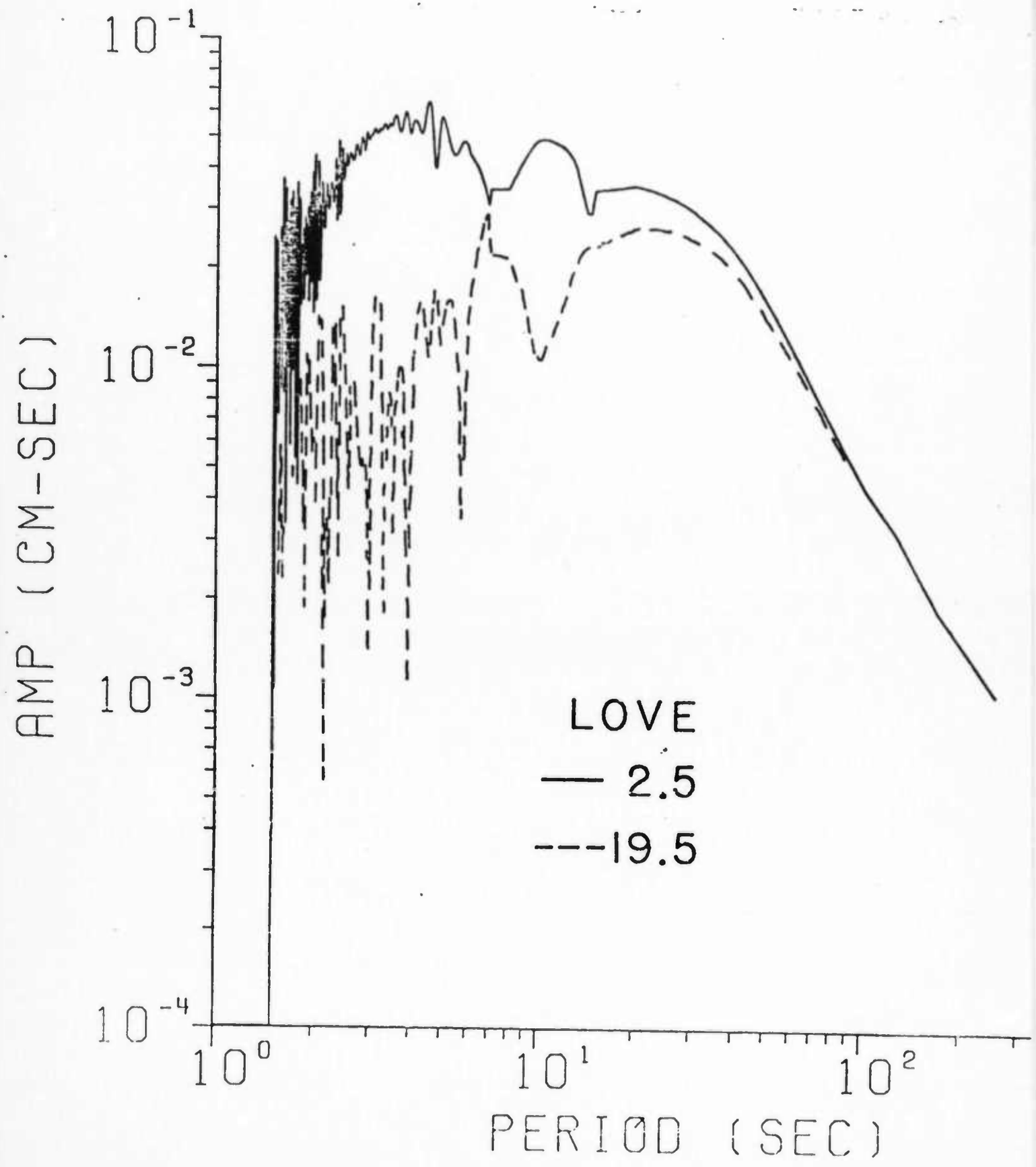

Figure 3

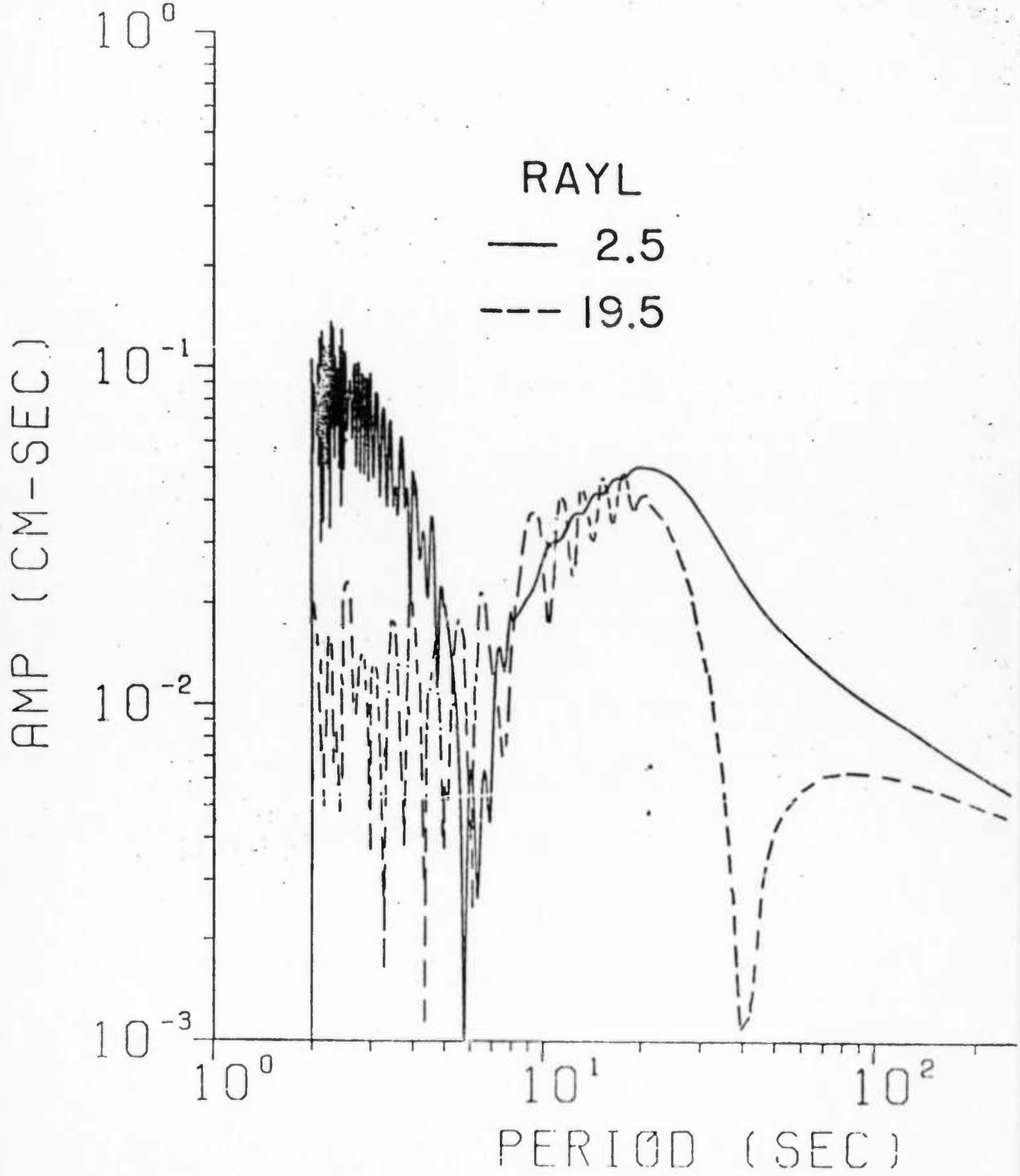

Figure 4

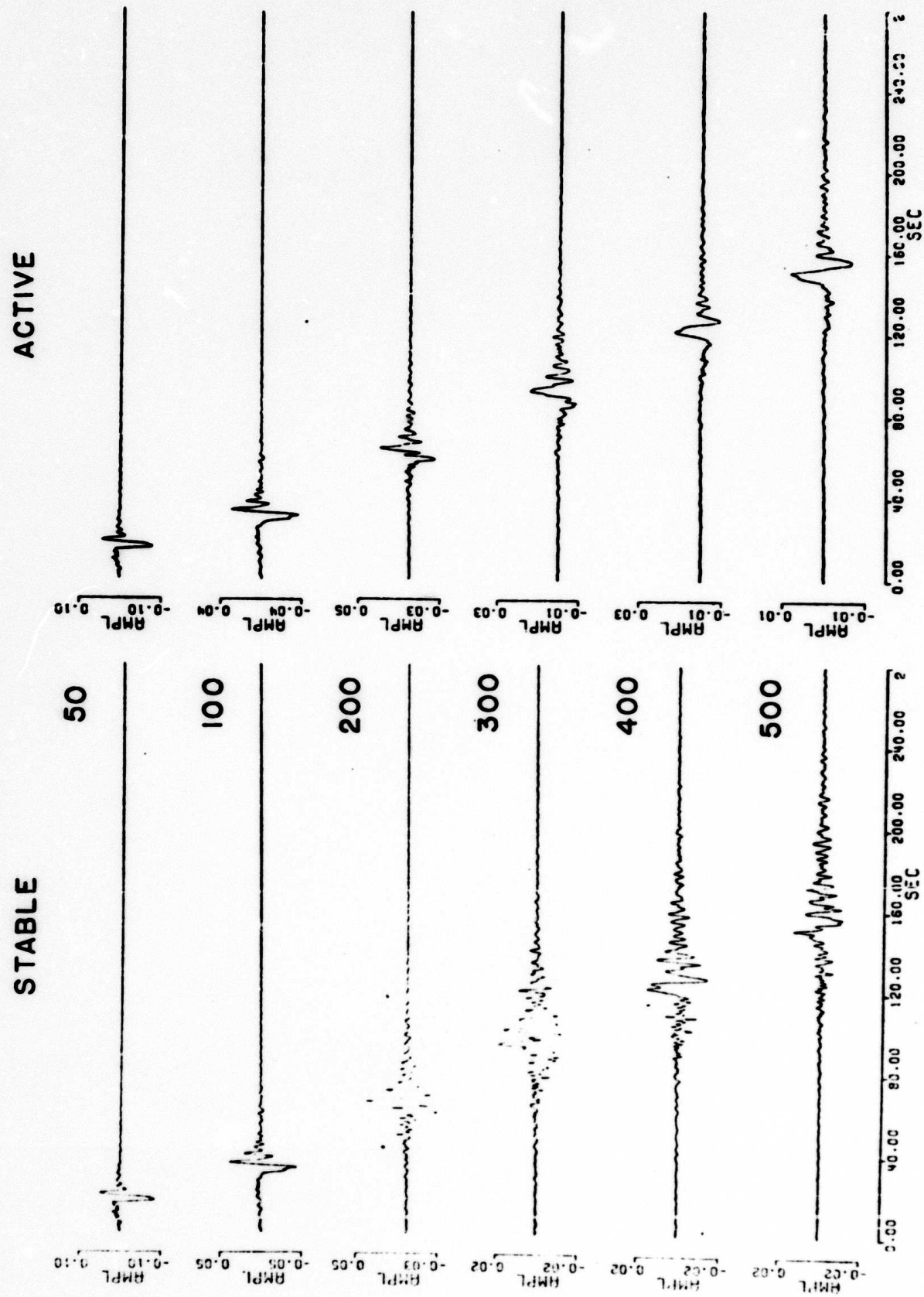

Figure 5

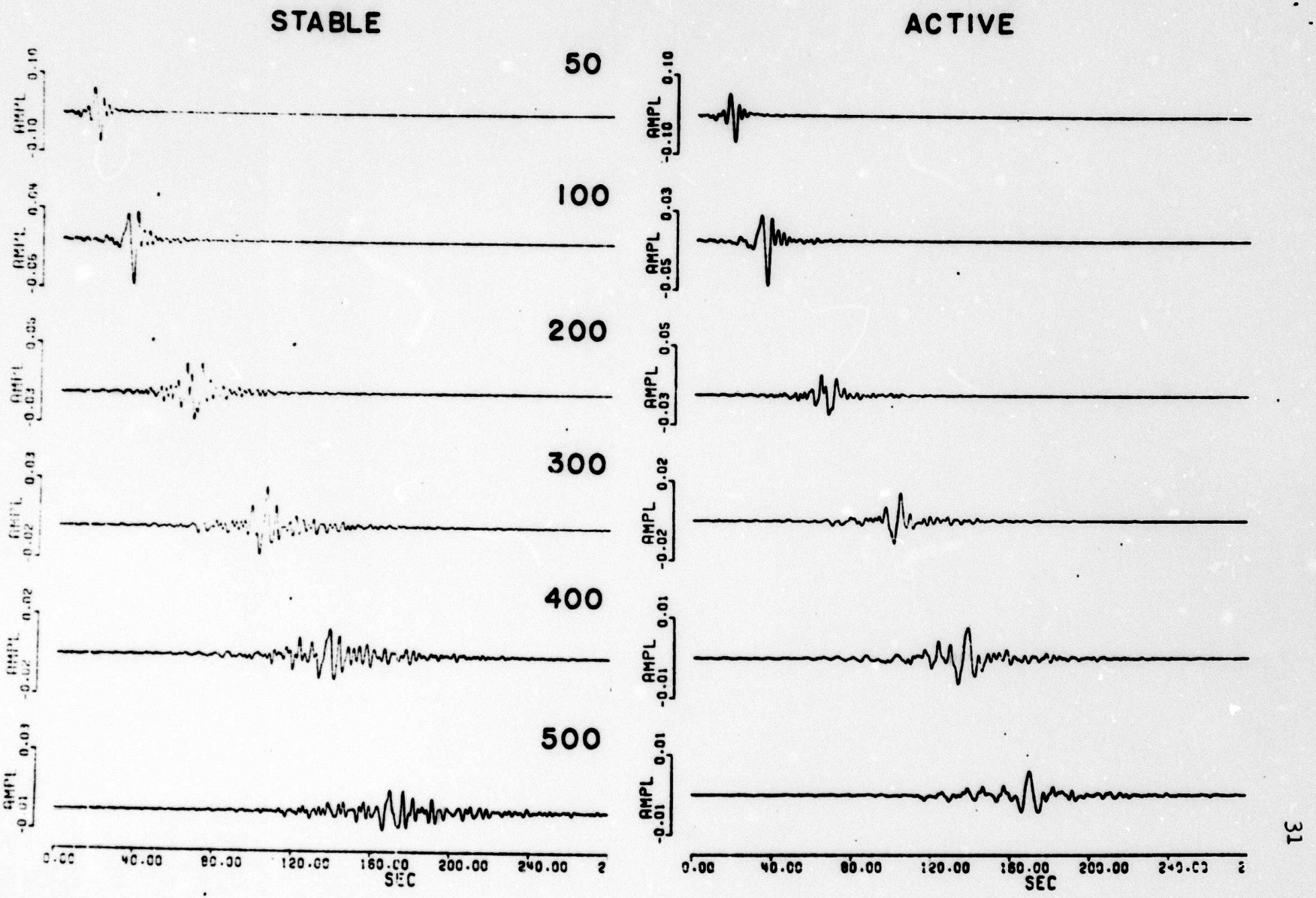
STABLE
ACTIVE
50
100
200
300
400
500
AMPL
-0.10
0.10
-0.05
0.03
-0.03
0.05
-0.02
0.02
-0.01
0.01
0.00
40.00
80.00
120.00
160.00
200.00
240.00
SEC

Figure 6

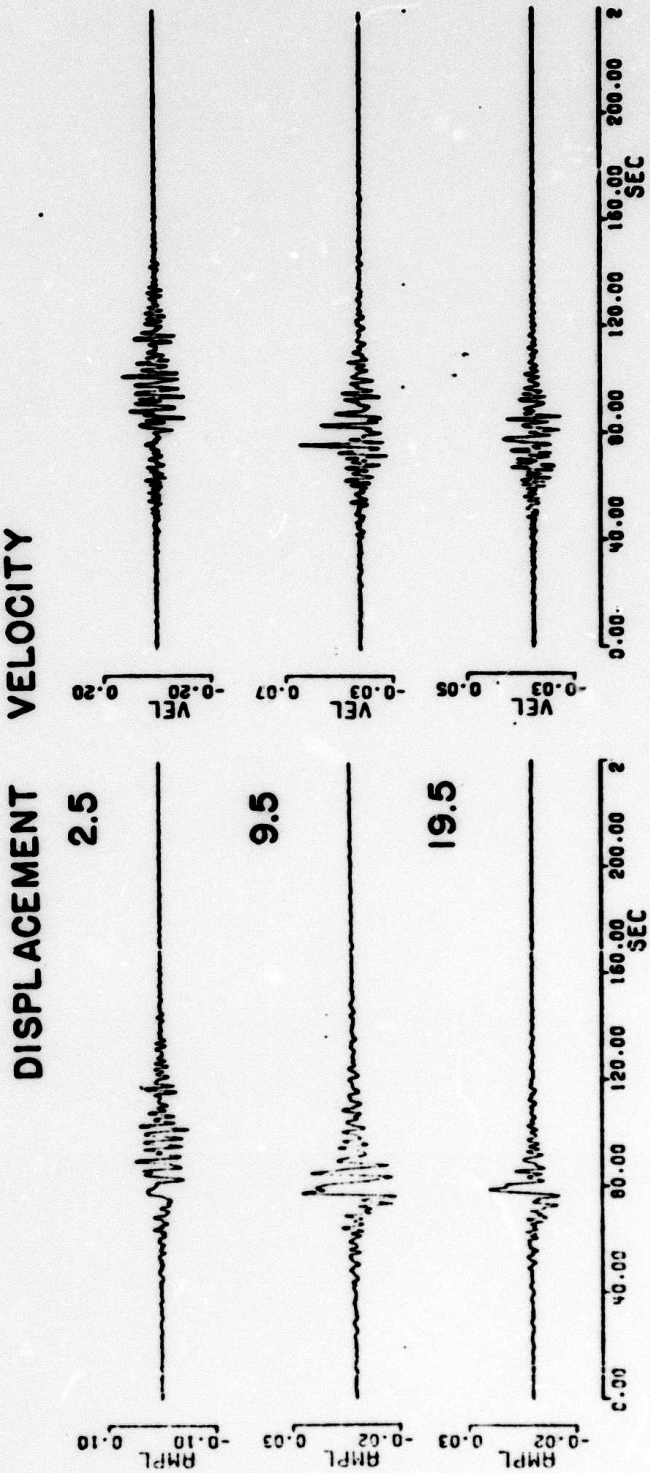
DISPLACEMENT
VELOCITY
2.5
9.5
19.5
RMPL
VEL
SEC
0.00
40.00
80.00
120.00
160.00
200.00

Figure 7

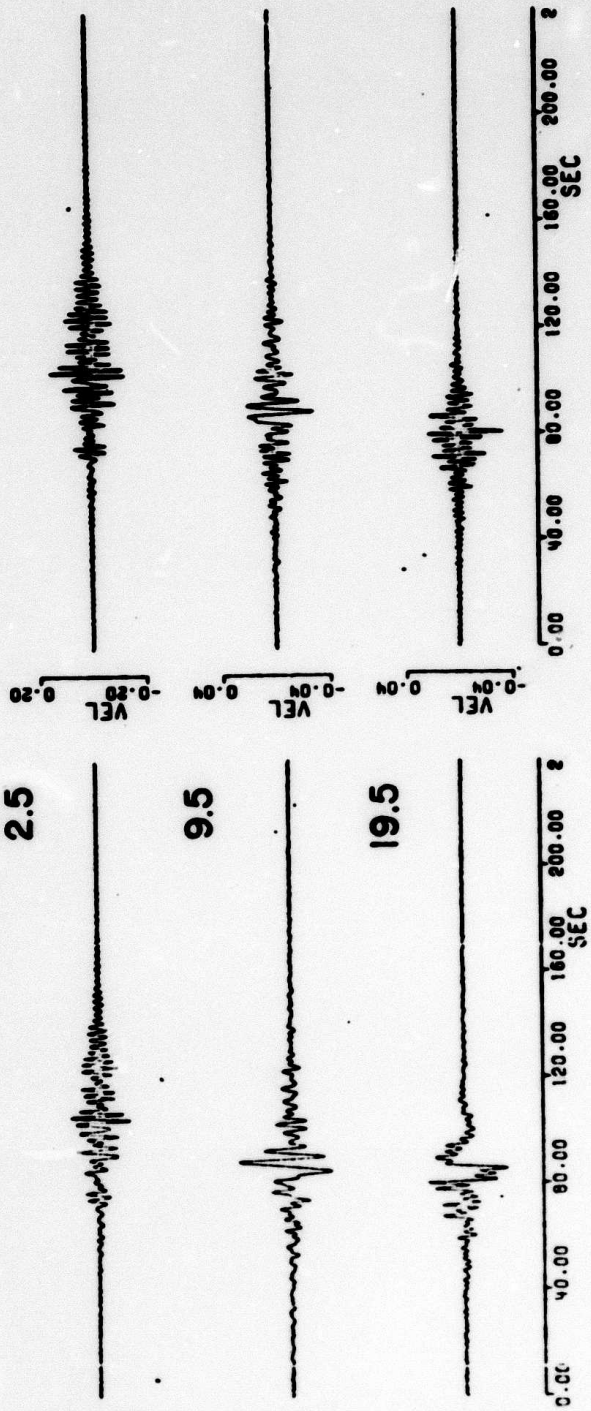
DISPLACEMENT
VELOCITY
2.5
9.5
19.5
AMPL
VEL
SEC
0.00
40.00
80.00
120.00
160.00
200.00

Figure 8

A. 3. Regional Rayleigh Wave Attenuation in North America

by Brian J. Mitchell

Introduction

Surface wave velocities and their regional variations have been studied extensively. Few studies have been made, however, of the attenuation of these waves, and there is almost no information on the regional variation of surface wave attenuation.

The present study seeks to investigate regional variations in surface wave attenuation by considering eastern and western North America separately. Various studies, including measurements of travel times (Hales et al, 1968), geomagnetic variations (Porath, 1971), and heat flow (Roy et al, 1972) indicate a rapid lateral change in properties of the crust and upper mantle near a line separating the Cordillera and Great Plains of North America. Two nuclear events, Rulison and Rio Blanco, were detonated in western Colorado, not greatly distant from that boundary. Rayleigh waves propagating eastward and westward from those events provide a means for investigating differences in Rayleigh wave attenuation for the two provinces described above.

Effect of Velocity Structure on Attenuation.

Anderson et al (1965) present a theory for the attenuation of dispersed waves. They determine quality factors for Love and Rayleigh waves in terms of the quality factors for compressional and shear waves and partial derivatives of Love and Rayleigh wave phase velocities with respect to shear and compressional wave velocities. Surface wave attenuation coefficient values are

related to the surface wave Q values through the equation $\gamma = \pi/UTQ$, where γ is the surface wave attenuation coefficient, U is the surface wave group velocity, Q is the surface wave quality factor, and T is the period. γ, U, and Q may refer to either Love or Rayleigh waves.

It is convenient for the present problem to reformulate the equations of Anderson et al (1965) in terms of surface wave attenuation coefficients rather than quality factors. The equations then become

$$\gamma_L = \frac{\pi}{C_L T} \sum_{\ell=1}^{N} \left(\frac{\partial Q_L^{-1}}{\partial Q_{\beta\ell}} \right)_\omega Q_{\beta\ell}^{-1}$$

$$= \frac{\pi}{T} \sum_{\ell=1}^{N} \left(\frac{\beta_\ell}{C_L^2} \frac{\partial C_L}{\partial \beta_\ell} \right)_{\omega\rho} Q_{\beta\ell}^{-1} \qquad (1)$$

$$\gamma_R = \frac{\pi}{C_R T} \sum_{\ell=1}^{N} \left[\left(\frac{\partial Q_R^{-1}}{\partial Q_{\alpha\ell}^{-1}} \right) Q_{\alpha\ell}^{-1} + \left(\frac{\partial Q_R^{-1}}{\partial Q_{\beta\ell}^{-1}} \right) Q_{\beta\ell}^{-1} \right]_\omega$$

$$= \frac{\pi}{T} \left[\sum_{\ell=1}^{N} \left(\frac{\alpha_\ell}{C_R^2} \frac{\partial C_R}{\partial \alpha_\ell} \right)_{\omega\rho\beta} Q_{\alpha\ell}^{-1} + \sum_{\ell=1}^{N} \left(\frac{\beta_\ell}{C_R^2} \frac{\partial C_R}{\partial \beta_\ell} \right)_{\omega\rho\alpha} Q_{\beta\ell}^{-1} \right] \qquad (2)$$

where α and β are compressional- and shear-wave velocities, Q_α and Q_β are the quality factors for compressional and shear waves, C_L and C_R are Love and Rayleigh wave phase velocities, and ℓ is a layer index. The subscripts ω, α, β, and ρ refer to the frequency, compressional velocity, shear velocity, or density being held constant.

Partial derivatives of Rayleigh wave phase velocity with respect to compressional and shear velocities were computed for models taken to be representative of the central United States

(McEvilly, 1965) and the Colorado Plateau (Bucher and Smith, 1971). Figure 3 depicts these two models and the Rayleigh wave phase velocities which they produce. The greatest differences in the phase velocities occur at periods less than 5 seconds, the Colorado Plateau model being much slower than the central United States model for those periods. At greater periods, the Colorado Plateau velocities parallel and lie somewhat below those of the central United States.

The application of equations (1) and (2) requires the partial derivatives discussed above and appropriate values for Q_α and Q_β. Two simple 2-layer Q models were selected and Rayleigh wave attenuation coefficients were computed using equation (2). At depths greater than 17 km both models possessed constant Q_β values of 2000. At shallow depths, one model consisted of material with a Q_β value of 200 and the other had a Q_β value of 100. These are simplified forms of an earlier model determined by Mitchell (1973b). The Q_α values were taken to be twice as great as the Q_β values, using the relationships determined by Anderson et al (1965) for the mantle, and assuming they also apply to the crust. Surface waves are much less sensitive to Q_α than to Q_β.

Knowledge of the attenuation coefficients permits one to calculate the effect on amplitudes, since $A \propto \exp[-\gamma(\omega)x]$. The distance, x, was taken to be 1000 km, and the amplitude factor, $\exp[-\gamma(\omega)x]$, was computed for the Colorado Plateau and central United States velocity models (Figure 3), combined with the two Q models described above. Figure 4 presents the results of the computations. Although the velocity structure produces differences of more than 2 orders of magnitude at a period of 1 second, it has very little effect at periods of 5 seconds and more.

Although the two velocity models differ throughout their depth, the greatest differences occur in the uppermost few km, where low velocity sediments are present in the Colorado Plateau model and absent in the central United States model. The short-period Rayleigh wave energy travelling across the Colorado Plateau model concentrates in the faster, deeper material rather than the low-velocity sediments.

The Rayleigh wave radiation patterns at a period of 2 seconds in Figures 1 and 2 indicate very large amplitudes to the north and northeast and smaller amplitudes to the west, south and southeast. The large amplitudes were recorded at stations in the Canadian shield and northeastern United States where sediments are either thin or absent, whereas smaller amplitudes were recorded by stations with thicker accumulations of sediments, such as the western United States and Gulf coastal plain.

Rayleigh Wave Attenuation Coefficients.

For a near surface composite of an explosion and double-couple source with approximately the same source-time functions, the far-field vertical displacement for a Rayleigh wave can be written

$$W_R(\omega) = W_e(\omega)\left[1 + F(\omega)\sin 2(\theta - \theta_o)\right] \exp\left[-\gamma(\omega)x\right] \qquad (3)$$

where W_e represents the vertical displacement produced by an explosion, F is the relative strength of the double couple, θ_o is the orientation of the double couple, γ is the Rayleigh wave attenuation coefficient, and x and θ are the distance and azimuth from the source, respectively (Toksöz et al, 1971).

Values for W_e, F, θ_o and γ can be determined at each period by fitting equation (3) to the observed data by a least-squares

iterative process. Equation (3) strictly refers to a composite of an explosion and a horizontal double-couple source. The horizontal double-couple can be taken to represent a vertical strike-slip fault (Toksöz and Kehrer, 1972), in which case Θ_o will be the strike of the fault (or the auxiliary plane) and F will be the amount of tectonic strain release relative to the explosion. Although equation (3) represents a somewhat special case, the amplitude radiation patterns can assume a variety of shapes, depending on the values of F and Θ_o . The patterns are elliptical or two-lobed when F is less than 1.0, and four-lobed when F is greater than 1.0. Considering the scatter in amplitude data, most theoretical and observed patterns can be brought into satisfactory agreement with appropriate values of F and Θ_o . The attenuation coefficient value, γ , can consequently be correct even though the representation of the source as a composite explosion and vertical strike-slip fault may be incorrect.

The mean determinations of γ , W_e, F and Θ_o and their standard deviations for data from Rulison and Rio Blanco appear in Figures 5 and 6. The fit of the theoretical patterns to the observations, using these values, are shown in Figures 1 and 2.

We are most interested in values of the Rayleigh wave attenuation coefficient, γ . They decrease from about 0.8×10^{-3} km^{-1} at a period of 5 seconds to very small or slightly negative values at periods of 12-14 seconds, and assume a roughly constant value of about 0.05×10^{-3} at greater periods. Results of the following section will indicate that regional variations in Q_β structure substantially affect Rayleigh wave attenuation to periods at least as great as 16 seconds. The regional variations

are reflected by large standard deviations, however, only at periods less than 8 or 9 seconds. Non-random as well as random effects must therefore be operative on the observations at periods less than about 16 seconds. Non-random effects probably produce the negative attenuation coefficient values at periods of 12-14 seconds. This can be explained in terms of the average path lengths from the sources to eastern or western North American stations. On the average, paths to western stations are substantially shorter than paths to eastern stations. Since attenuation is greater to the west than to the east from the sources, the net effect is to produce low apparent attenuation coefficient values. Consequently, all of the observed attenuation coefficient values for periods less than 16 seconds will be lower than the actual average values.

Comparative Attenuation for Eastern and Western North America

It was described earlier how we would divide North America into two provinces, one east of the Cordillera-Great Plains boundary, and the other to the west. The amplitudes recorded for surface waves which have travelled entirely within each of these provinces are now considered separately. Disregarding those observations which do not clearly represent one of the two provinces, average amplitudes are determined for the eastern (A_W) and western province (A_E) for each period. The average ratios of the values, A_W/A_E, appear in Figure 7. At periods of 18 seconds and greater, the values are only slightly less than unity. At shorter periods, the values decrease with decreasing period to a value of about 0.2 at a period of 7 seconds.

These amplitude ratios lead to values for attenuation coefficient differences through the relation

$$\gamma_W - \gamma_E = -\frac{\ln(A_W/A_E)}{X} \qquad (4)$$

where γ_W and γ_E are average attenuation coefficient values for western and eastern North America, respectively. Differences in anelasticity ($\frac{1}{Q}$) models can then be investigated by equations analogous to (3) and (4). For differences in Rayleigh wave attenuation coefficients we can write

$$\gamma_W - \gamma_E \cong \frac{\pi}{T}\left[\sum_{\ell=1}^{N}\left(\frac{a_\ell}{c_R^2}\frac{\partial c_R}{\partial a_\ell}\right)_{\omega\beta\rho}\Delta(Q_{a\ell}^{-1}) + \sum_{\ell=1}^{N}\left(\frac{\beta_\ell}{c_R^2}\frac{\partial c_R}{\partial \beta_\ell}\right)_{\omega\rho a}\Delta(Q_{\beta\ell}^{-1})\right] \qquad (5)$$

The validity of this approximation requires that the first factors in each term have about the same values for the two models considered. For periods of 5 seconds and greater, equation (5) was found to be applicable. If we assume that $Q_\alpha = 2\,Q_\beta$, as discussed above, equation (5) becomes

$$\gamma_W - \gamma_E \cong \frac{\pi}{T}\sum_{\ell=1}^{N}\left[\left(\frac{\beta_\ell}{c_R^2}\frac{\partial c_R}{\partial \beta_\ell}\right)_{\omega\rho a} + \frac{1}{2}\left(\frac{a_\ell}{c_R^2}\frac{\partial c_R}{\partial a_\ell}\right)_{\omega\rho\beta}\right]\Delta(Q_{\beta\ell}^{-1}) \qquad (6)$$

This equation permits a determination of the difference in the Q_β^{-1} distribution for two different models using the data of Figure 7. As stated above, we will consider the two models to be the two large provinces of North America, overlooking smaller scale variations within each province.

The basic theory for inverse problems permitting the consideration of errors and resolution was developed by Backus and Gilbert (1970). The present inversion problem is particularly simple since it is a linear one. The method of solution is discussed by Mitchell (1973b).

The results of two inversions appear in Figure 8. The solid line permits a very good fit to the data of Figure 7, whereas the dashed line is a solution for which the theoretical values differ from the observed values by about 30 per cent at short periods. The main features of both curves are the same. The resolving kernels on the right side of Figure 8 indicate the degree of resolution for $\Delta (Q_\beta^{-1})$ at the indicated depth in the model. Narrow peaks, well-localized at the proper depths, indicated by the vertical dashes, imply a high degree of resolution, whereas broad, poorly-localized peaks imply poor resolution. At a depth of 2 km, the peak is narrow, but poorly localized. The localization improves below 2 km, but the kernels broaden rapidly at depths greater than 15 km.

If a Q_β model for eastern North America is available, or assumed, one can determine an average Q_β model for western North America by using the results presented in Figure 8. The only crustal Q_β model available at the present time is that of Mitchell (1973b). The solid line in Figure 9 is a slight simplification of that model for eastern North America. The dashed line in Figure 9 is a Q_β model for western North America determined from a modification of the ENA 7 model of Mitchell (1973b) and the values indicated in Figure 8. The average values of Q_β for the upper crust of western North America are about half those of model ENA 7. At greater depths, the model is less reliable

because of the poor resolution in the determination of $\Delta(Q_\beta^{-1})$ at those depths.

Effect of Temperature on Attenuation.

One of the results of the present study is that values for Q_β in the upper crust of North America, in gross terms, are about half those of eastern North America. The reason for this difference is not clearly known, although temperature differences for the two regions provide one possible mechanism. This possibility can be examined by considering the variation of Q_β in a homogeneous material as being due to variations of temperature (T) and pressure (P) only. This situation can be expressed by

$$Q_\beta^{-1}(T,P) = Q_o^{-1} \exp\left[E^*(T-T_o)/RT_oT\right] \exp\left[-PV^*/RT\right] \qquad (7)$$

where E* and V* are the activation energy and activation volume, and Q_o^{-1}, and T_o refer to reference values of quality factor and temperature. If we consider two regions which differ only by their temperature distribution, we can write for the difference in anelasticity between the two regions

$$\Delta(Q_\beta^{-1}) = Q_{oW}^{-1} \exp\left[E^*(T_W-T_o)/RT_oT_W\right] \exp\left[-PV^*/RT_W\right]$$
$$- Q_{oE}^{-1} \exp\left[E^*(T_E-T_o)/RT_oT_E\right] \exp\left[-PV^*/RT_E\right] \qquad (8)$$

where the subscripts E and W refer to the eastern and western North American models. Equation (8) can be solved for T_W to obtain

$$T_W = \frac{E^*(T_E/T_0 - 1) - P}{R \ln\left\{Q_{0W}\,\Delta(Q_\beta^{-1}) + \frac{Q_{0W}}{Q_{0E}} \exp\left[E^*(T_E - T_0)/RT_0T_E\right] \exp\left[-PV^*/RT_E\right]\right\}} \qquad (9)$$

This expression can be used to determine values for E* and V* which satisfy the temperatures as a function of depth for the two regions, assuming that homogeneous material is the same for each region. Values of $\Delta(Q_\beta^{-1})$, Q_{oW} and Q_{oE} are taken from Figures 8 and 9. Thermal models for the eastern United States and Basin and Range province are given by Blackwell (1971). These are taken to be representative of the thermal structures of the two large provinces discussed above, for purposes of computation, although the temperatures in the Basin and Range Province are probably slightly higher than average for western North America.

The temperature ratios, T_W/T_E , determined from the values of Blackwell (1971) are shown as a dashed line in Figure 10. The value for the activation volume has little effect at crustal depths; consequently only an appropriate value for the activation energy, E*, was required. Temperature ratios for various values of E* appear in Figure 10. It appears that a value of 1.7 kcal/mole could adequately explain the Q_β differences for eastern and western North America in terms of temperature alone. However, this result pertains to the relative values $\Delta(Q^{-1})$. If the same value of E* is applied to equation (7) for either an eastern or western North American model alone, the Q_β values decrease very rapidly with depth to values less than 50 at a depth of 20 km. These are much too small to satisfy the attenuation data; consequently differences in Q_β in the upper crust of eastern and

western North America cannot be explained solely by lateral variations in temperature within a homogeneous material. Differences in the lower crust could, however, still be explained by temperature differences.

References

Anderson, D. L., A. Ben-Menahem, and C. B. Archambeau, Attenuation of seismic energy in the upper mantle, J. Geophys. Res., 70, 1441-1448, 1965.

Backus, G., and F. Gilbert, Uniqueness in the inversion of inaccurate gross earth data, Phil. Trans. Roy. Soc. (London), Ser. A, 266, 123-192, 1970.

Blackwell, D. D., The thermal structure of the continental crust, in The Structure and Physical Properties of the Earth's Crust, edited by J. G. Heacock, 169-184, 1971.

Bucher, R. L., and R. B. Smith, Crustal structure of the eastern Basin and Range province and the northern Colorado plateau from phase velocities of Rayleigh waves, in The Structure and Physical Properties of the Earth's Crust, edited by J. G. Heacock, 59-70, 1971.

Hales, A. L., J. R. Cleary, H. A. Doyle, R. Green, and J. Roberts, P-wave station anomalies and the structure of the upper mantle, J. Geophys. Res., 73, 3885-3896.

McEvilly, T. V., Central U. S. crust-upper mantle structure from Love- and Rayleigh-wave phase velocity inversion, Bull. Seism. Soc. Am., 54, 1997-2015, 1964.

Mitchell, B. J., Radiation and attenuation of Rayleigh waves from the southeastern Missouri earthquake of October 21, 1965, J. Geophys. Res., 78, 886-899, 1973.

Mitchell, B. J., Surface wave attenuation and crustal anelasticity in central North America, Bull. Seism. Soc. Am., 63, 1057-1071, 1973.

Porath, H., Magnetic variation anomalies and seismic low-velocity zone in the western United States, J. Geophys. Res., 76, 2643-2648, 1971.

Roy, R. F., D. D. Blackwell, and E. R. Decker, Continental Heat Flow, in The Nature of the Solid Earth, edited by E. C. Robertson, 506-543, 1972.

Toksoz, M. N., and H. H. Kehrer, Tectonic strain release by underground nuclear explosions and its effect on seismic discrimination, Geophys. J. R. Ast. Soc., 31, 141-161, 1972.

Toksoz, M. N., K. C. Thomson, and T. J. Ahrens, Generation of seismic waves by explosions in prestressed media, Bull. Seism. Soc. Am., 61, 1589-1623, 1971.

Figure Captions

Figure 1. Amplitudes of Rayleigh waves generated by Rulison (dots) and theoretical radiation patterns for a composite explosion and double-couple source. The four short lines in each diagram indicate an amplitude of 1.0×10^{-3} cm-sec.

Figure 2. Amplitudes of Rayleigh waves generated by Rio Blanco (dots) and theoretical radiation patterns for a composite explosion and double-couple source. The four short lines in each diagram indicate an amplitude of 2.0×10^{-3} cm-sec.

Figure 3. Compressional velocities (α), shear velocities (β), and densities (ρ) for models of the central United States and Colorado Plateau and the Rayleigh wave phase velocity curves which they produce.

Figure 4. Amplitude factors, $e^{-\gamma x}$, for the models of Figure 3. Q_1 indicates the Q_β value in the upper 17 km of the crust. Q_β for the lower crust was taken to be 2000 in all cases.

Figure 5. Average values of Rayleigh wave amplitude attenuation coefficient (γ), ground motion produced by the explosion (W_e), relative strength of the double couple component relative to the explosion (F), and orientation of the double couple for the Rulison event. The vertical bars represent the value of the standard deviation for each determination.

Figure 6. The quantities described in Figure 5 for the Rio Blanco event.

Figure 7. The ratio of average amplitudes recorded west and east of the sources. The solid and dashed lines result from the two models of Figure 8.

Figure 8. Values of (Q_β^{-1}) resulting from the solution of equation (6). The solid line produces a very good fit to the data of Figure 7 and the dashed line produces amplitude ratio values which differ from the observations by about 30 per cent at short periods. Resolving kernels for several depths appear on the right.

Figure 9. A modification of Q_β model ENA 7 (Mitchell, 1973b) for eastern North America (solid) and a model for western North America (dashed) based upon ENA 7 and the values of Figure 8.

Figure 10. Ratios of temperature needed to produce differences between eastern and western North American Q_β models for various values of activation energy (solid lines), and ratios derived from thermal models of the eastern United States and Basin and Range province (dashed line).

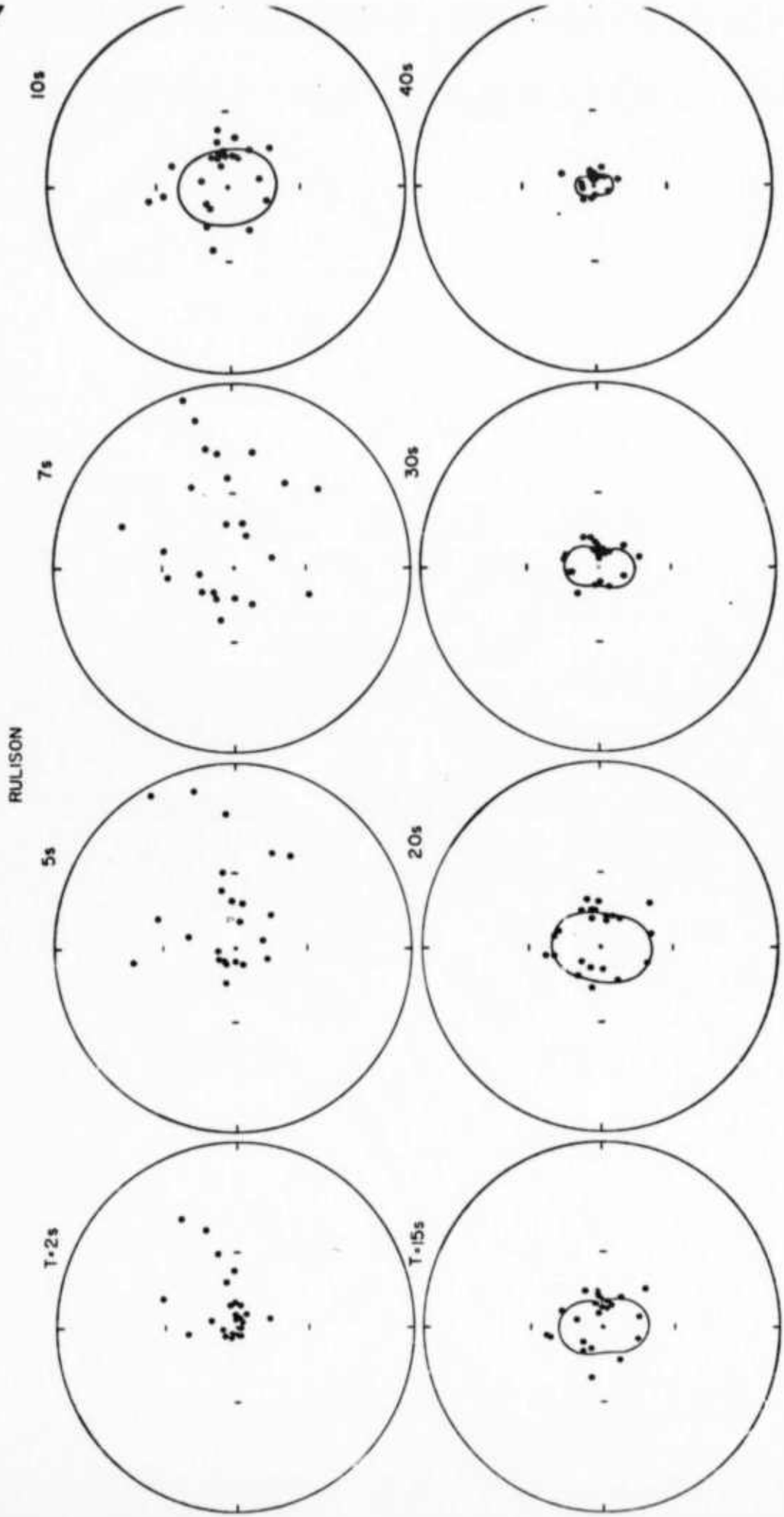

Figure 1

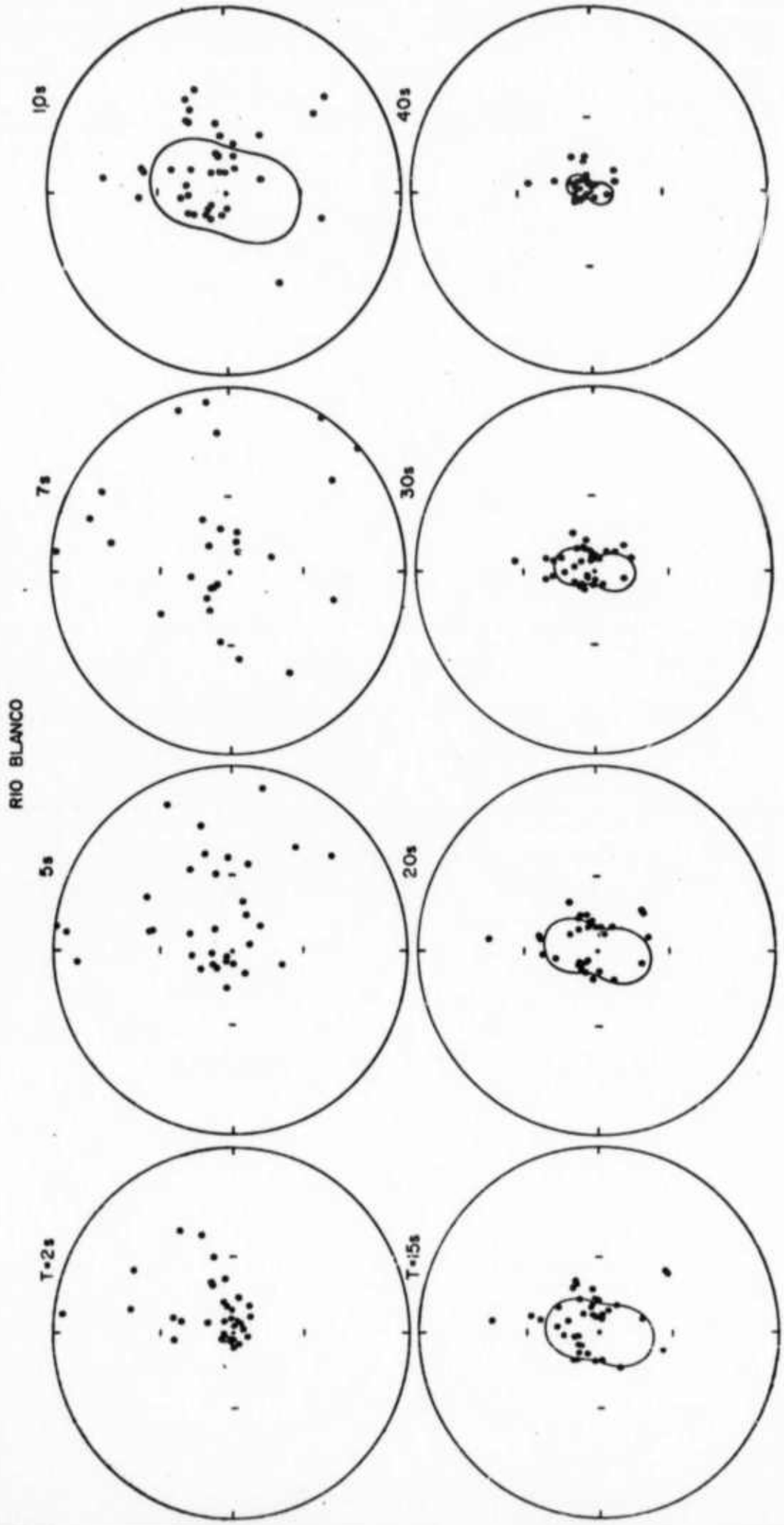

Figure 2

Depth, km	CENTRAL U.S. α	CENTRAL U.S. β	CENTRAL U.S. ρ	COLORADO PLATEAU α	COLORADO PLATEAU β	COLORADO PLATEAU ρ
0	6.10	3.50	2.70	3.00	1.73	2.40
10	6.40	3.68	2.90	6.20	3.58	2.83
20	6.70	3.67	2.90	6.80	3.87	2.99
30	8.15	4.67	3.30	7.80	4.25	3.30
40	8.20	4.47	3.30	8.20	4.38	3.43
50						
60						
70						
80						
90						
100						

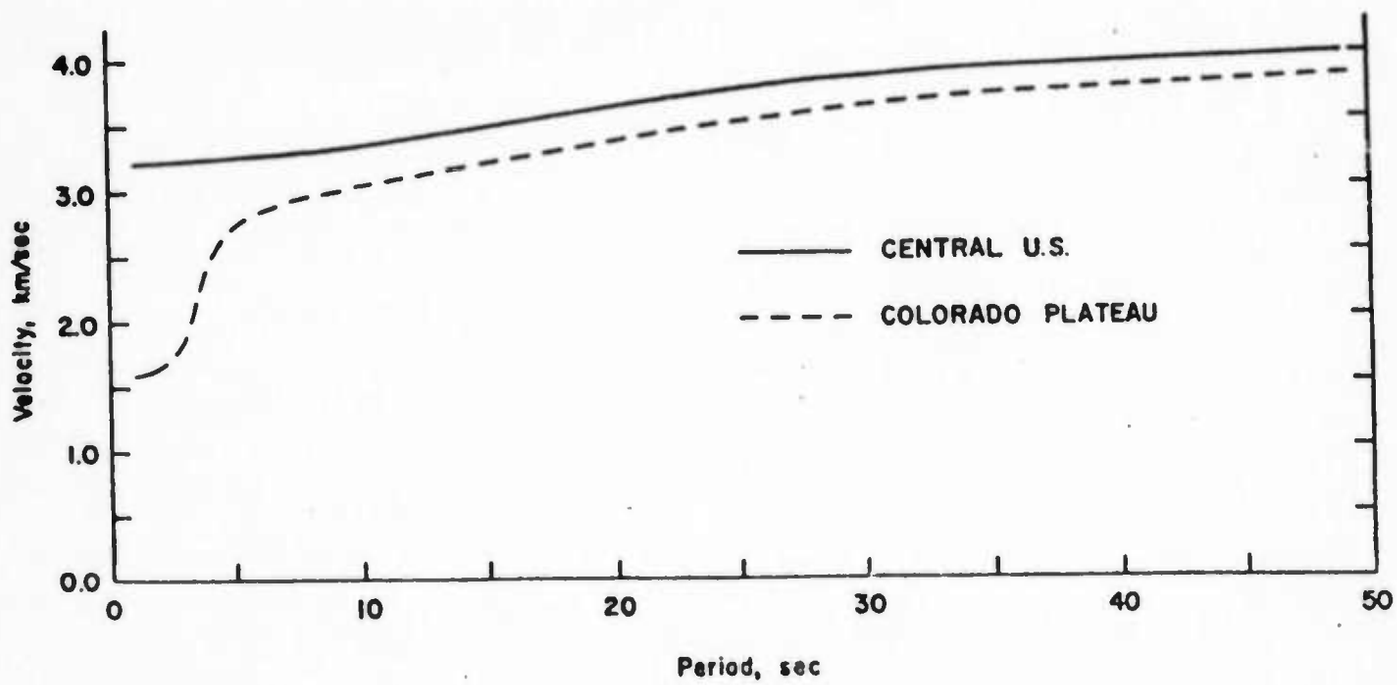

Figure 3.

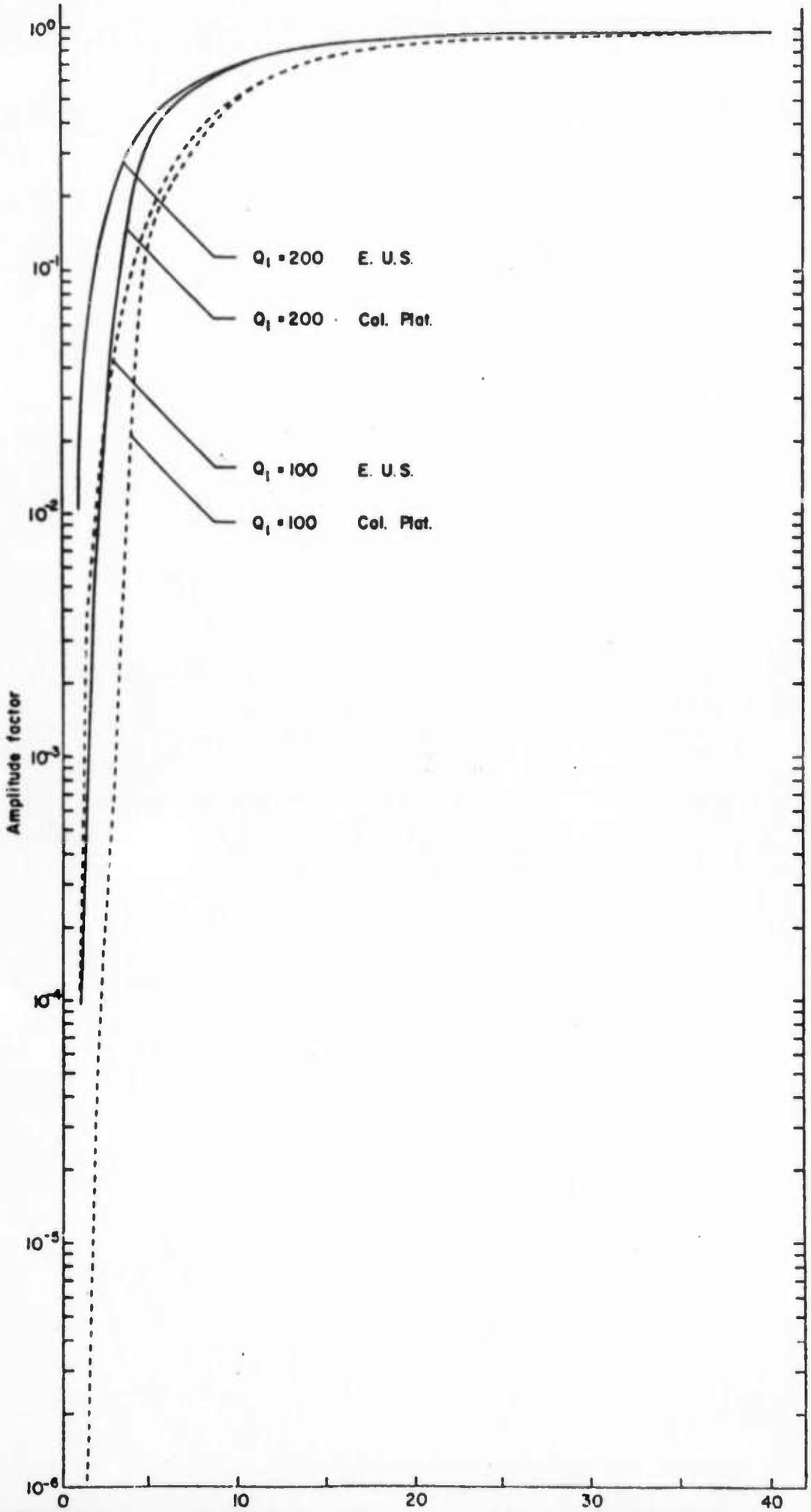
10^{0}
10^{-1}
10^{-2}
10^{-3}
10^{-4}
10^{-5}
10^{-6}
Amplitude factor
$Q_1 = 200$ E. U.S.
$Q_1 = 200$ Col. Plat.
$Q_1 = 100$ E. U.S.
$Q_1 = 100$ Col. Plat.
0
10
20
30
40

Figure 4.

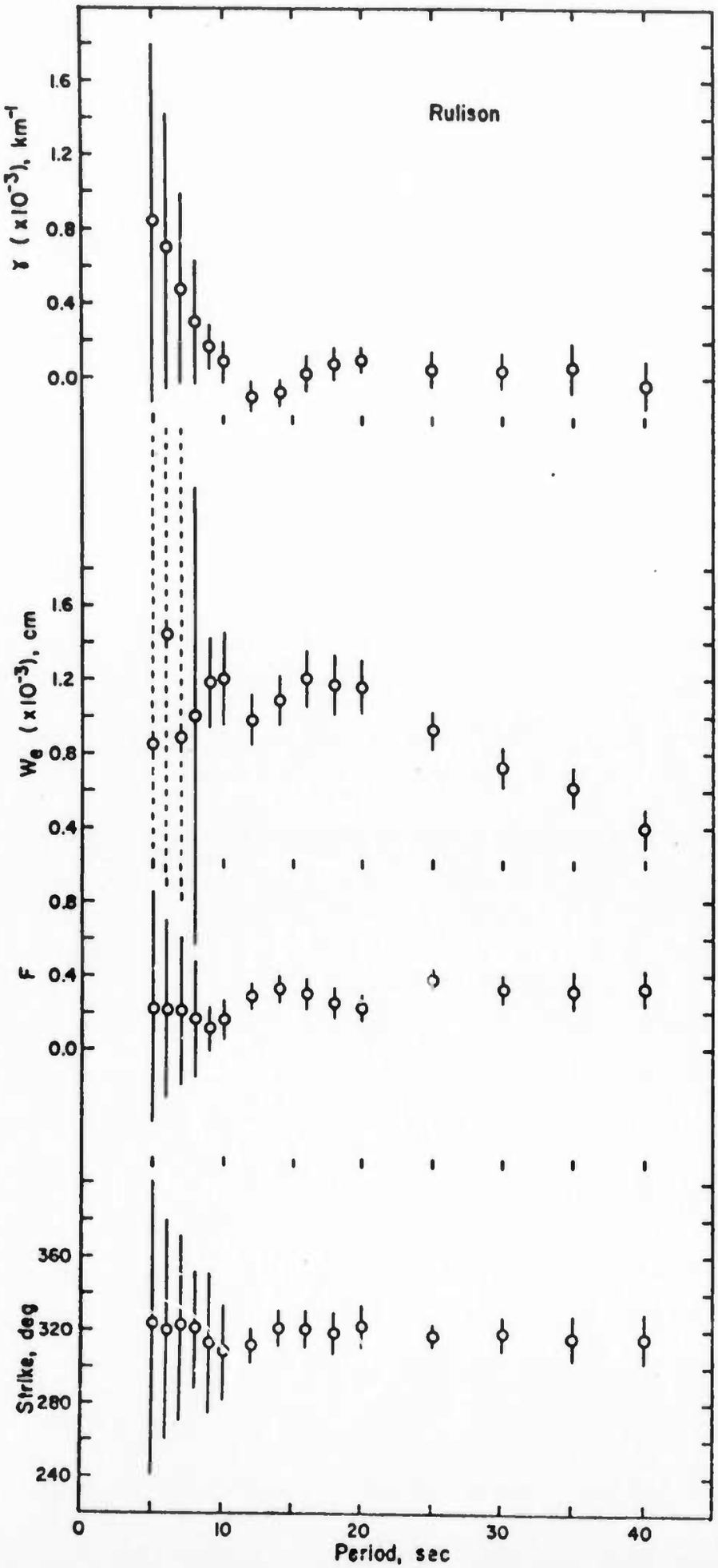
Rulison
γ (x10⁻³), km⁻¹
1.6
1.2
0.8
0.4
0.0
We (x10⁻³), cm
1.6
1.2
0.8
0.4
F
0.8
0.4
0.0
Strike, deg
360
320
280
240
0
10
20
30
40
Period, sec

Figure 5.

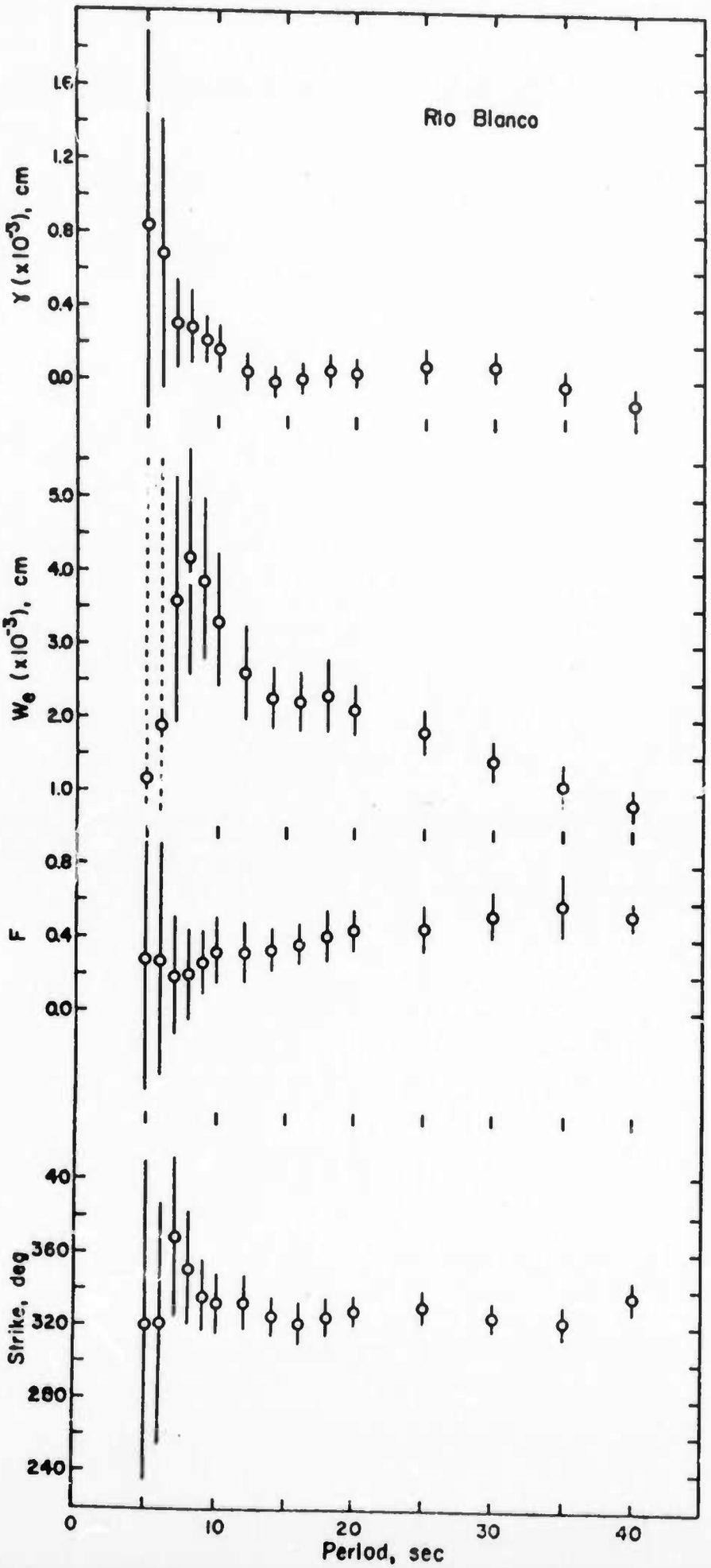
Rio Blanco
Y (x10⁻³), cm
1.6
1.2
0.8
0.4
0.0
We (x10⁻³), cm
5.0
4.0
3.0
2.0
1.0
F
0.8
0.4
0.0
Strike, deg
40
360
320
280
240
0
10
20
30
40
Period, sec

Figure 6.

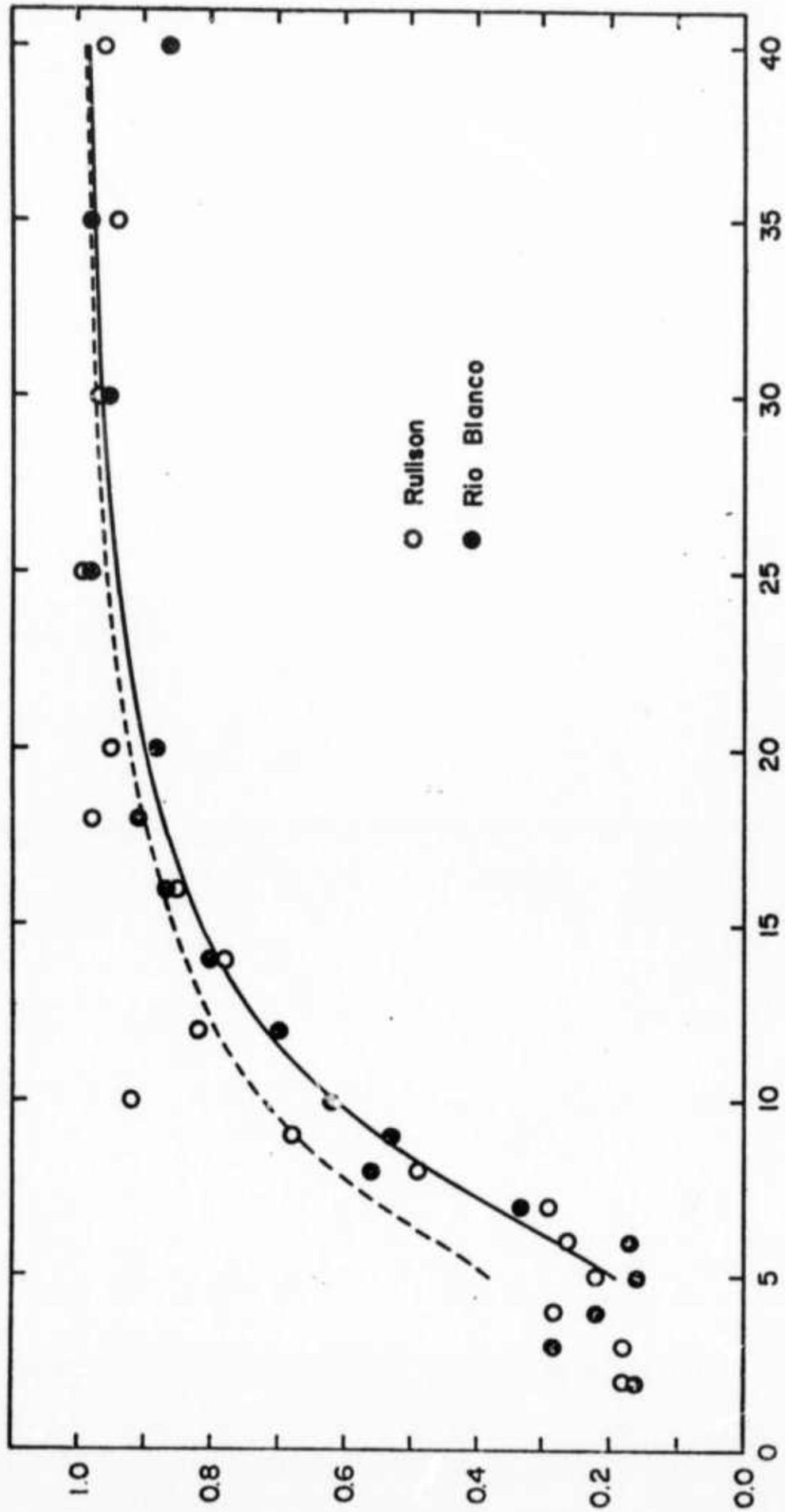
Amplitude ratio (west/east)
0.0
0.2
0.4
0.6
0.8
1.0
0
5
10
15
20
25
30
35
40
Period, sec
Rulison
Rio Blanco

Figure 7

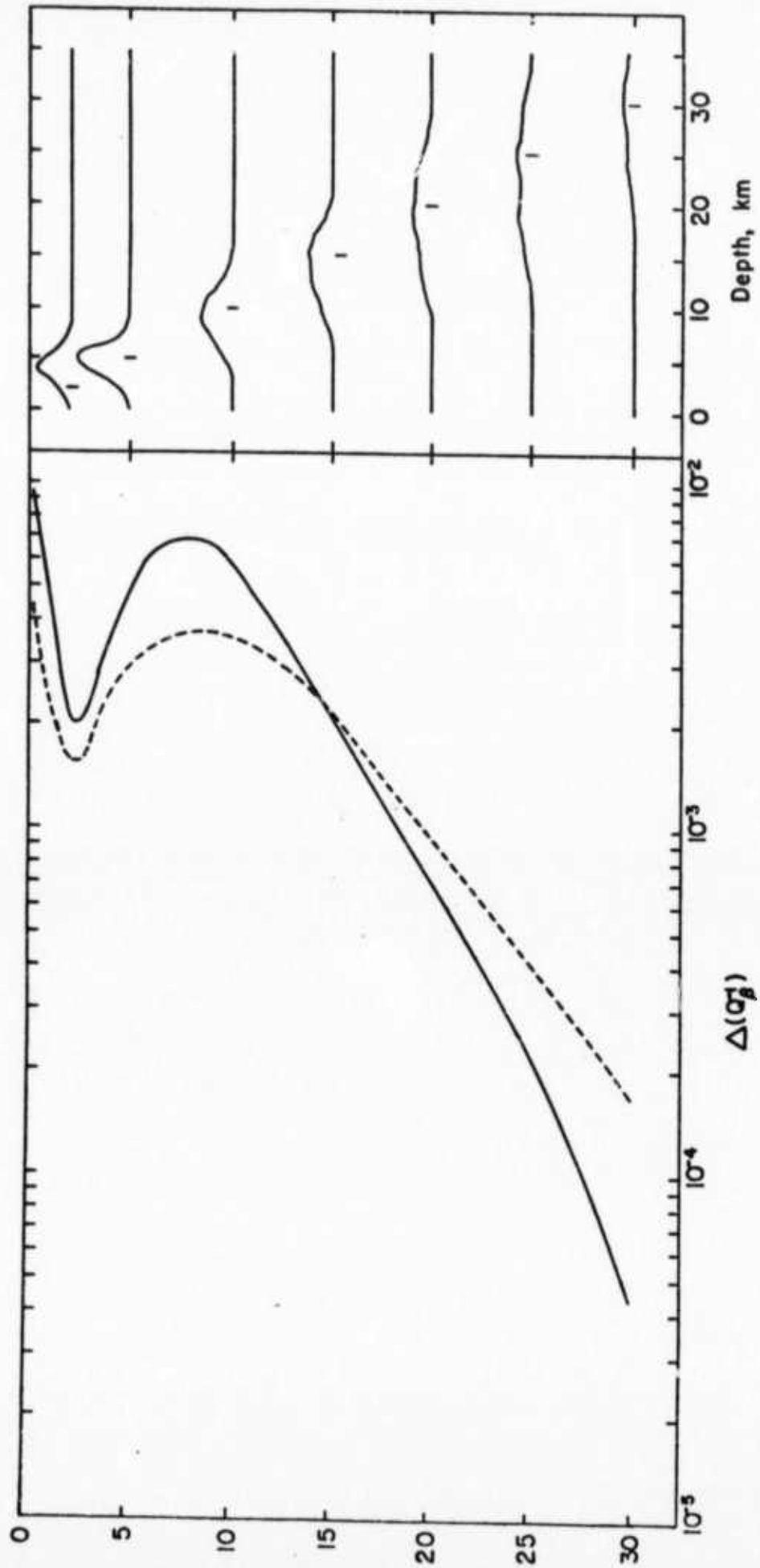
Depth, km
0
5
10
15
20
25
30
10^{-5}
10^{-4}
10^{-3}
10^{-2}
$\Delta(\sigma_\beta')$
Depth, km
0
10
20
30

Figure 8

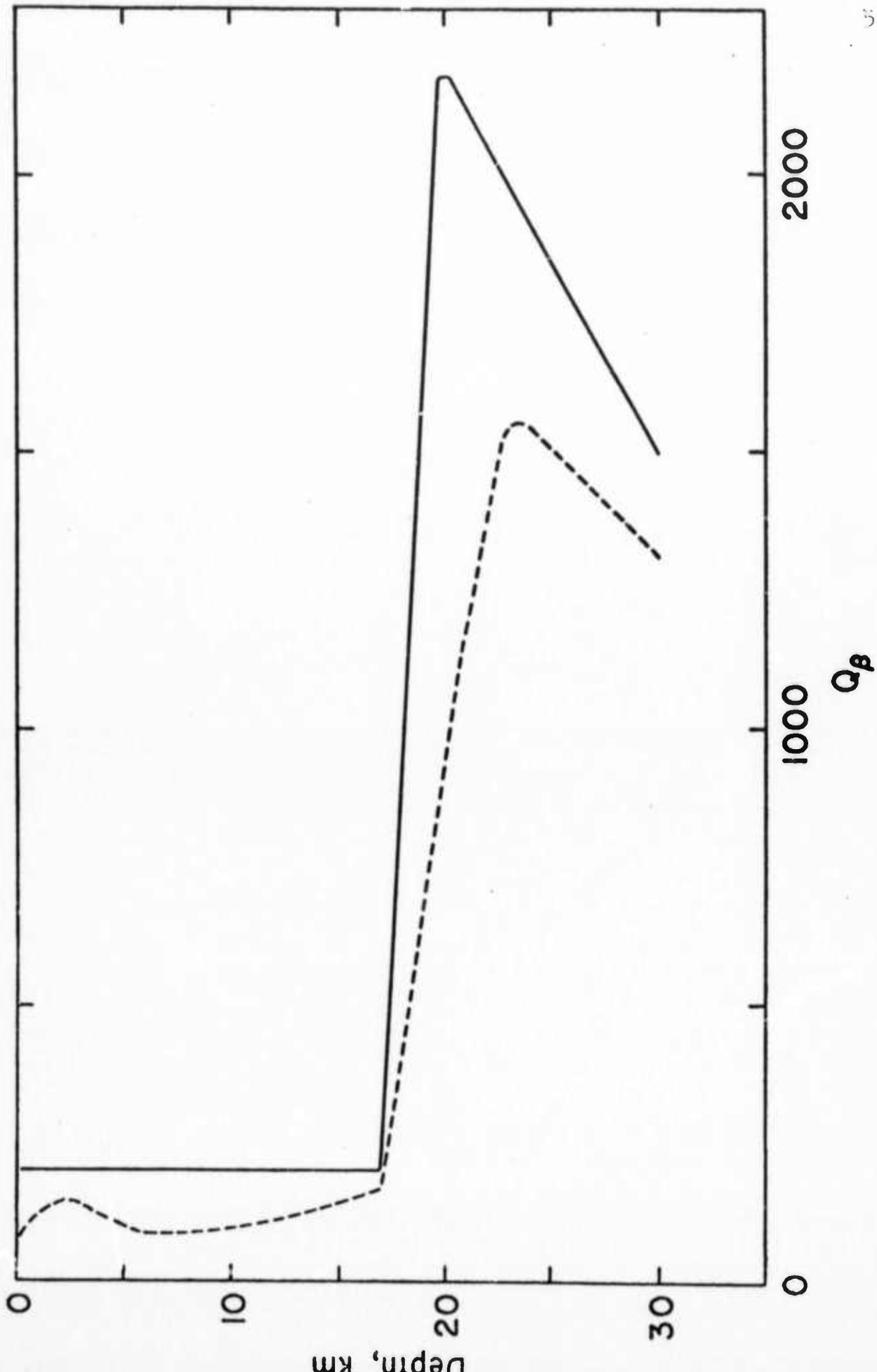

Figure 9

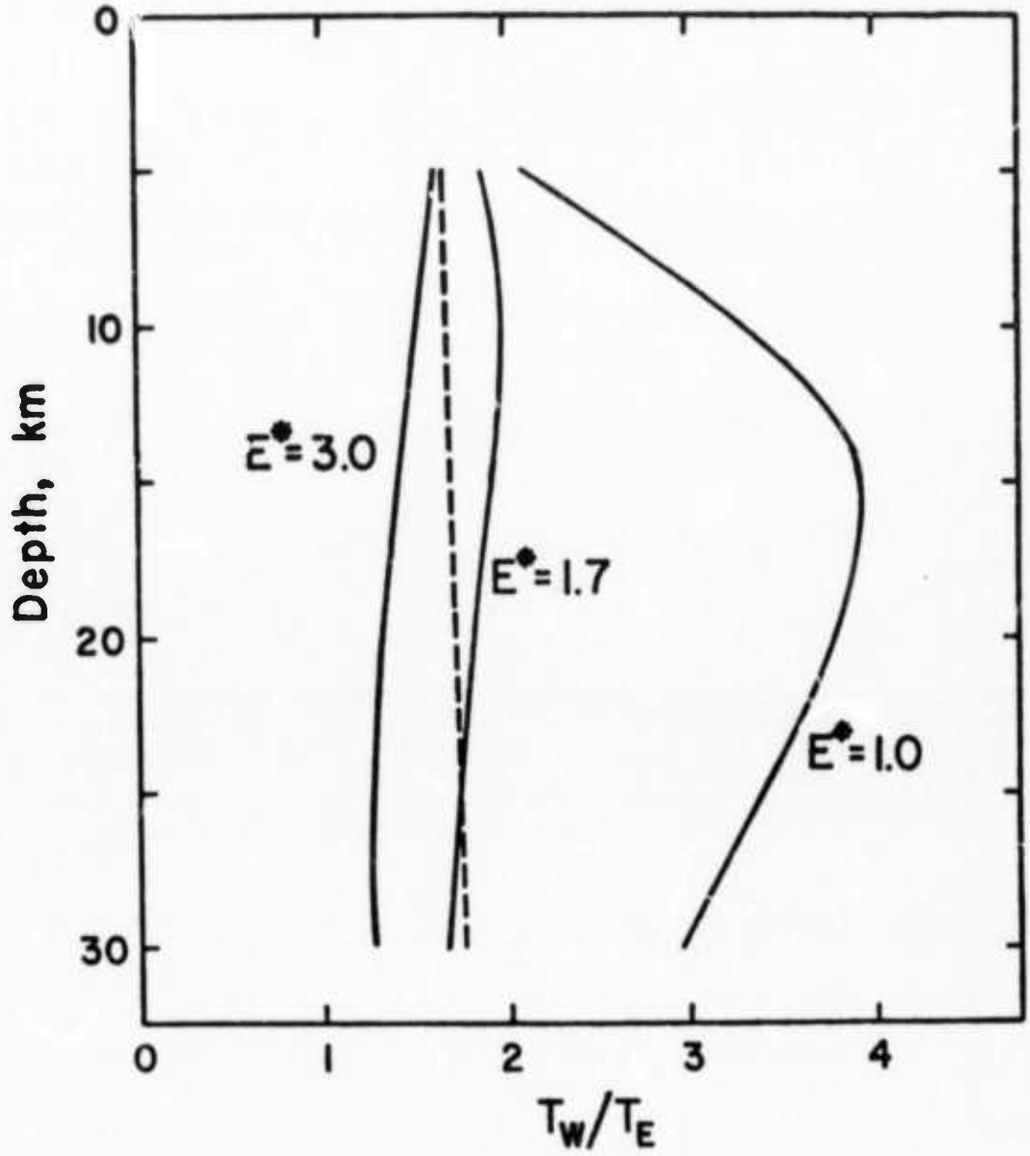

Figure 10.

B. Work in Progress

Work in progress includes two studies, one of the surface wave attenuation in Eurasia, the other of the radiation of seismic waves from shallow sources in the Sakhalin and Kurile Islands.

B. 1. Surface Wave Attenuation in Eurasia

Introduction

Surface wave attenuation coefficients determine the rate at which surface wave energy dissipates as it travels away from an earthquake or an explosion. Values for the observed attenuation coefficients are determined in ideal cases by the intrinsic Q values of the materials through which the waves travel. In real cases, however, attenuation is also produced by scattering, lateral refraction, and mulipathing produced by non-ideal source conditions, geologic complexities, and lateral variation of velocity and attenuative properties of the medium.

For the reasons cited above, attenuation data are more difficult to obtain than velocity data, and consequently the amount of attenuation data presently available, especially in certain regions, are quite limited. The Eurasian continent is one of the regions for which surface wave attenuation data are limited. The only presently available data for sources in Eurasia are those of Tryggvason (1965) and Burton (1974). Both of these studies, however, include paths which traverse both continental and oceanic regions; their results consequently may not pertain to true attenuation within Eurasia.

The present work will restrict both sources and stations to the Eurasian continent. This approach avoids complications which arise from waves which travel through ocean basins or which cross

continental boundaries. The disadvantage of this approach is the relatively small number of stations available for the determination of attenuation coefficients.

We seek to determine attenuation coefficient values of periods between 10 and about 100 seconds. The shorter periods are especially affected by the complexities discussed above. The long path lengths from sources to seismograph stations in Eurasia combined with complexities along most paths lead to relatively large standard deviation values for average attenuation coefficient values in that region. Our approach will be to present these average values and their standard deviations, and then to look for regional departures from these average values.

Events

Data from nine events are presently in various stages of analysis. Table 1 lists these events in chronological order. The table includes six earthquakes, one underground nuclear explosion, and two atmospheric nuclear explosions. Surface waves from the earthquakes and underground explosion yield data in the period range from about 10 to 50 seconds, and surface waves from the atmospheric nuclear events extend these data to periods of about 100 seconds. We attempted to obtain a wide distribution of events throughout Eurasia. We were limited, however, by the absence of useful events over much of the region under study.

Stations

Stations of the World Wide Standard Seismograph Network (WWSSN) have provided most of the data used in the present work.

Data from stations of the USSR have been ordered through World Data Center A but have not arrived in the several months since the order.

The absence of WWSSN in the USSR and China limits most of the available data from eastern Asia to paths through the southern portions of the continent. The Novaya Zemla nuclear events do, however, provide a few paths further to the north in eastern Asia.

The Geophysical Institute in Peking, China, has provided film copies of seismograms produced by the events of November 8, 1971 and November 18, 1971. The records are from Kirnos type instruments with a flat response between 0.3 and 12 seconds. Data from these will therefore be limited to relatively short periods.

Method

The method for obtaining attenuation coefficient values is that of Mitchell (1974). It assumes chat any event can be considered as an explosion plus a horizontal double couple component and can be described by

$$A(\omega) = W_e \left[1 + F \sin 2(\theta - \theta_o)\right] \exp\left[-\gamma(\omega)x\right] \qquad (1)$$

where $A(\omega)$ is the spectral amplitude, W_e is the component of motion due to an explosion, F is the ratio of energy due to the double couple as compared to an explosion, θ_o is the orientation of the double couple, γ is the attenuation coefficient, x is the distance between the source and receiver, and θ is the azimuthal direction from the source. The quantities W_e, F, and θ_o are functions of frequency (ω) and have physical meaning only when the source is a composite of an earthquake and an explosion.

It is found that patterns of spectral amplitudes described by equation (1) can assume circular, elliptical, two-lobed, or four lobed shapes, depending on the value of F. Consequently, most any radiation pattern produced by explosions or earthquakes can be described by the equation. Values for W_e, F, Θ_o, and γ can be determined from a least-squares fit between observed and theoretical radiation patterns at each period. Although W_e, F, and Θ_o will not have physical meaning except in special cases, γ will be the true attenuation coefficient in all cases.

Results to date

The Chinese nuclear event of September 9, 1969, the Chinese earthquake of November 1, 1971, the U.S.S.R. earthquake of October 28, 1971, the U.S.S.R earthquake of November 18, 1971 have yielded average Rayleigh wave attenuation coefficient values. In each case the values are characterized by greater standard deviation values than those obtained from work in North America. A relatively small number of available stations and long paths over geologically complex regions probably combine to produce these standard deviations.

The Chinese earthquake produces low values for the Rayleigh wave attenuation coefficient over the entire period range between 10 and 50 seconds. The values range from slightly negative to about 0.03×10^{-3} km^{-1} and have standard deviations of about 0.2×10^{-3}. The Chinese nuclear event produces values which are similar to those above between 10 and 50 seconds, but extends the range of data to about 100 seconds. The Rayleigh wave attenuation coefficient values remain low to periods of 70 seconds,

then appear to increase to about 0.3×10^{-3} at a period of 100 seconds. The standard deviation through most of the period range is about 0.1×10^{-3}.

The Russian earthquakes exhibit higher values, but within the error limits all of the values are similar. The values for these cases decrease from about 0.6×10^{-3} km^{-1} at a period of 10 seconds to about 0.2×10^{-3} km^{-1} at a period of 20 seconds and remain nearly constant out to a period of 50 seconds. The standard deviations are about 0.2×10^{-3} for most of the period range.

Some of the values listed above may change if we can supplement our present data set with data from stations in the U.S.S.R.

Regional variations in attenuation seem to occur, especially at the shorter periods. Consistently high amplitudes are recorded by stations in Fennoscandia and are probably due to relatively low attenuation across the Baltic shield. Lower than average amplitudes occur at Asian stations for paths across the Himalayas and Tibeten Plateau. It is uncertain as yet whether these low values are due to intrinsically lower Q values in the region or to scattering effects.

References

Burton, P.M., Estimations of Q^{-1} from seismic Rayleigh waves, Geophys. J. R. Ast. Soc., 36, 167-189, 1974.

Mitchell, B. J., Regional Rayleigh wave attenuation in North America, submitted 1974.

Tryggvason, E., Dissipation of Rayleigh wave energy, J. Geophys. Res., 70, 1449-1455, 1965.

Table 1

Date	Origin time	Type of event	Geographic Coordinates		Country
Sept. 27, 1962	08 03 15.4	Atmospheric Explosion	74.3N	52.4E	USSR
July 11, 1968	10 02 05.3	Underground Explosion	73.4N	54.9E	USSR
Sept. 9, 1969	08 40 31.0	Atmospheric Explosion	40.7N	89.6E	China
Aug. 16, 1971	18 53 54.7	Earthquake	28.9N	103.7E	China
Oct. 10, 1971	18 25 14.6	Earthquake	23.0N	96.0E	Burma
Oct. 28, 1971	13 30 57.1	Earthquake	41.9N	72.4E	USSR
Nov. 1, 1971	05 29 57.2	Earthquake	44.0N	85.1E	China
Nov. 8, 1971	03 06 36.4	Earthquake	27.1N	54.5E	Iran
Nov. 18, 1971	07 31 32.8	Earthquake	38.3N	66.8E	USSR

B. 2. Radiation from Shallow Focus Earthquakes in the Sakhalin and Kurile Islands.

A sequence of six earthquakes, a main shock and five of its larger aftershocks, occurring in the Sakhalin Islands in September 1971 have been selected for study. The depths of focus for these earthquakes vary from 6 km to 24 km. Focal mechanism solutions have been determined for each, and have been found to vary from almost pure thrust motion in the main shock to a progressively more dominant strike slip motion in the aftershocks.

The dates of occurrence, locations, and focal parameters of these earthquakes are given in Table 1.

With the determination of the focal mechanisms as a base, work is now in progress in comparing the M_S vs m_b values, particularly at Eurasian stations. This will be followed by a study of the computed and observed spectral characteristics to examine to what extent the shallow depth of focus and thrust mechanism may affect determinations of M_S.

Other examples of shallow thrust fault earthquakes in the Kurile Islands (Stauder and Mualchin, 1974) are available and will be used in comparison with, and in supplementing information from, the Sakhalin Islands earthquakes.

Reference

Stauder, W., and L. Mualchin, Fault motion in larger earthquakes of the Kurile-Kamchatka Arc and of the Kurile-Hokkaido Corner, submitted to J. Geophys. Res.

Table 1. Focal Parameters of Sakhalin Island Earthquakes.

Date	Origin	Lat.	Long.	h	m_b	X		Y		B		P		T	
						Tr	Pl	Tr	Pl	Tr	Pl	Tr	Pl	Tr	Pl
5 Sep 71	18-35-25.0	46.5N	141.2E	9	6.3	300°	47°	100°	41°	199°	10°	290°	3°	36°	79°
6 Sep 71	06-45-59.0	46.6	141.1	16	5.7	315	45	90	35	199	24	290	5	32	65
6 Sep 71	13-37-10.8	46.7	141.4	29	6.1	300	48	100	40	199	10	289	4	41	79
8 Sep 71	11-48-23.4	46.4	141.1	6	5.9	315	22	60	32	196	49	99	6	4	40
8 Sep 71	16-59-52.6	46.3	140.9	16	5.9	315	28	70	38	198	39	104	6	7	50
27 Sep 71	19-01-45.3	46.4	141.1	21	5.9	320	27	65	27	192	50	282	0	13	40